NASA CR—159416
SRD-78-191

NASA-CR-159416
19790012051

EVALUATION OF AN ADVANCED DIRECTIONALLY SOLIDIFIED γ/γ'-α Mo EUTECTIC ALLOY

by

M.F. Henry, M.R. Jackson, M.F.X. Gigliotti, and P.B. Nelson

January 1979

General Electric Company
Corporate Research and Development
Schenectady, New York 12301

Prepared for:

NATIONAL AERONAUTICS AND SPACE ADMINISTRATION

Lewis Research Center
Cleveland, Ohio 44135

Contract NAS 3-20383

FINAL REPORT

TECHNICAL REPORT STANDARD TITLE PAGE

1. Report No. NASA CR-159416	2. Government Accession No.	3. Recipient's Catalog No.
4. Title and Subtitle EVALUATION OF AN ADVANCED DIRECTIONALLY SOLIDIFIED γ/γ' - αMo EUTECTIC ALLOY		5. Report Date January 1979 6. Performing Organization Code
7. Author(s) M.F. Henry, M.R. Jackson, M.F.X. Gigliotti and P.B. Nelson		8. Performing Organization Report No. SRD-78-191
9. Performing Organization Name and Address Corporate Research and Development General Electric Company P.O. Box 43 Schenectady, New York 12305		10. Work Unit No. 11. Contract or Grant No. NAS 3-20383 13. Type of Report and Period Covered Contractor Report
12. Sponsoring Agency Name and Address National Aeronautics and Space Administration Lewis Research Center Cleveland, Ohio 44135		14. Sponsoring Agency Code

15. Supplementary Notes

Project Manager, F.H. Harf; Research Advisor, C.M. Scheuermann; NASA Lewis Research Center, Cleveland, Ohio

16. Abstract

The purpose of this program was to improve on the properties of the candidate jet engine turbine blade material AG-60, a γ/γ'-α Mo eutectic composite. Of the 39 alloys considered in this program, alloy 38 (AG-170) was evaluated in the greatest detail. This alloy, Ni-5.88 Al-29.74 Mo-1.65 V-1.20 Re (weight percent), represents an improvement beyond AG-60, based on mechanical testing of the transverse and/or longitudinal orientations over a range of temperatures in tension, shear, rupture, and rupture after thermal exposure. It is likely that other alloys in this study represent a similar improvement.

To more fully characterize the potential of γ/γ'-α Mo eutectics for turbine blade applications, further evaluations were performed on alloy 38. Thermal expansion and dynamic modulus measurements were made over a range of temperatures, cyclic oxidation resistance was determined, tensile and rupture properties were determined for coated test bars, creep resistance was measured, and blade shape processing was defined in terms of liquid metal/mold and core ceramic reactivity. After the coating heat treatment cycle, the rupture life of the alloy was 550 hours at 750°C/880 MPa, 150 hours at 950°C/300 MPa, and 425 hours at 1100°C/125 MPa. Although a number of problem areas remain to be treated, eutectics in the γ/γ'-α Mo system should be considered further as possible alternate or superior blade materials in comparison to the NiTaC and γ/γ'-δ eutectic systems.

17. Key Words (Selected by Author(s))	18. Distribution Statement
Eutectic alloys, Heat resistant alloys, High temperature tests, Nickel base alloys, Solidification	Unclassified - unlimited

19. Security Classif. (of this report)	20. Security Classif. (of this page)	21. No. of Pages	22. Price
Unclassified	Unclassified	73	

FOREWORD

This final technical report describes the work performed between November 30, 1976 and June 30, 1978 for the National Aeronautics and Space Administration Lewis Research Center under Contract No. NAS 3-20383, "Evaluation of an Advanced Directionally Solidified γ/γ'-αMo Eutectic Alloy." The report was prepared by the Metallurgy Laboratory of the General Electric Company's Research and Development Center in Schenectady, New York.

The experimental contributions of Arthur J. Peat were vital to the success of this study.

We are also indebted to the following contributors to this study: W.J. Baxter, M.G. Benz, C.F. Canestraro, M.F. Ciccarelli, P.L. Dupree, E.M. Habesch, Jr., F.S. Halsey, M. Heiberger, R.L. Mehan, W.F. Moore, C.P. Palmer, J.R. Rairden, T.F. Sawyer, W.A. Seaman, G.E. Stebbins, and P.S. Svec.

TABLE OF CONTENTS

Section		Page
1	SUMMARY	1
2	INTRODUCTION	3
3	MATERIALS AND PROCEDURES	9
	Melting	9
	Directional Solidification	9
	Structure Evaluation and Sectioning	10
	Density Determination	12
	Tensile Tests	12
	Longitudinal Shear Tests	15
	Creep and Stress Rupture Tests	15
	Thermal Cycling and Isothermal Exposures	15
	Cyclic Oxidation	16
	Ceramic/Metal Reactivity	16
	Thermal Expansion	16
	Dynamic Modulus	16
	Fluorescence Chemical Analysis	16
	Coating	17
4	RESULTS	19
	Preliminary Evaluation of Alloy Concepts	19
	Structure of Task I Alloys	19
	Stress Rupture Properties of Task-I Alloys	23
	Refinement of Alloy Concepts	26
	Structure of Task-II Alloys	27
	Tensile Properties of Task-II Alloys	28
	Stress Rupture Properties of Task-II Alloys	31
	Thermal Cyclical Effects on Stress Rupture Properties of Task-II Alloys	31
	Selection and Evaluation of Advanced γ/γ'-αMo Alloy	35
	Structure and Chemistry of Alloy 38	36
	Tensile and Shear Properties of Alloy 38	37
	Stress Rupture and Creep Properties of Alloy 38	39
	Effects of Prior Exposure on Stress Rupture Properties of Alloy 38	39
	Evaluation of Properties of Coated Alloy 38	41
	Thermal Expansion and Dynamic Modulus of Alloy 38	43
	Cyclical Oxidation Resistance of Alloy 38	43
	Casting and Reactivity Studies of Alloy 38	43

TABLE OF CONTENTS (Cont'd)

Section		Page
5	DISCUSSION OF RESULTS	49
	Physical Behavior	49
	Mechanical Properties	50
	Processing	52
6	CONCLUDING REMARKS	57
7	REFERENCES	59

LIST OF ILLUSTRATIONS

Figure		Page
1	Schematic Sectioning Diagram for Directionally Solidified Ingots	10
2	Visual Standards for Degree of Alignment in γ/γ'-αMo Longitudinal Sections	11
3	Visual Standards for Degree of Alignment in γ/γ'-αMo Transverse Sections	13
4	Specimen Used for Tensile and Creep Rupture Tests	14
5	Specimen Used for Longitudinal Shear Tests	14
6	Bar Chart of Task-I Stress Rupture Lives	25
7	Photomicrograph of Transverse Section of DS No. LDB-298 (Alloy 38) at 1 cm/h	29
8	Photomicrograph of Transverse Section of DS No. LDB-299 (Alloy 39) at 1 cm/h	29
9	Transverse Microstructure of Alloy 36	33
10	Transverse Microstructure of Alloy 28	34
11	Microstructures of IN-671-coated Alloy 38 After One-hour Exposures in Argon	42
12	Alloy 38 Casting DS No. LB-379 in Silica Bonded-alumina Mold	48

LIST OF ILLUSTRATIONS (Cont'd)

Figure		Page
13	Tensile Strength of Alloy 38 Compared to Other Eutectics for Longitudinal and Transverse Orientations	51
14	Longitudinal Shear Strength of Alloy 38 Compared to Other Eutectics	52
15	Rupture Behavior of Alloy 38 Compared to Other Eutectics for Longitudinal and Transverse Orientations	53

LIST OF TABLES

Table		Page
I	Property Goals for Eutectic Alloy Development	4
II	Composition of Task-I Alloys in Atomic Percent	20
III	Composition of Task-I Alloys in Weight Percent	21
IV	Structures of Task-I Alloys	22
V	Stress Rupture Results on Task-I Alloys	24
VI	Comparison of 36 Task-I Alloys and Base Alloy AG-60 in Stress Rupture Resistance in Vacuum	26
VII	Task-II Alloy Compositions and Growth Rates	27
VIII	Structure of Task-II Ingots	28
IX	Task-II Tensile Results at 750°C	30
X	Task-II Tensile Results at 1100°C	30
XI	Task-II Stress Rupture Results	32
XII	Task-II Thermal Cycling Results	32
XIII	Structure of Task-III Ingots of Alloy 38 at 1 cm/h, 4-cm Diameter	36
XIV	X-Ray Fluorescence Results for Alloy 38 Ingots	37
XV	Tensile Results for Alloy 38 at 1 cm/h	38
XVI	Longitudinal Shear Strength of Alloy 38 at 1 cm/h	38

LIST OF TABLES (Cont'd)

Table		Page
XVII	Stress Rupture Results for Alloy 38 at 1 cm/h	40
XVIII	Task-III Creep Tests of Alloy 38 at 1 cm/h	40
XIX	Longitudinal Stress Rupture Results for Alloy 38 at 1 cm/h After Prior Exposure	41
XX	Longitudinal Tensile Results for Alloy 38 at 1 cm/h	44
XXI	Longitudinal Stress Rupture Results for Alloy 38 at 1 cm/h	44
XXII	Longitudinal Thermal Expansion Data for Alloy 38 at 1 cm/h	45
XXIII	Longitudinal Dynamic (Sonic) Modulus for Alloy 38 at 1 cm/h	45
XXIV	Cyclical Oxidation Resistance of Alloy 38	46
XXV	Casting and Reactivity Studies of Alloy 38	46

Section 1

SUMMARY

The purpose of this program was to improve -- through changes in composition -- the Mo-fiber reinforced directionally solidified eutectic γ/γ'-α alloy (AG-60*) containing by weight 5.7 percent Al, 32.3 percent Mo, and the balance Ni, previously identified in contract NAS 3-19711. Since the scope of the properties important to blade design is too large to evaluate for a number of alloys, the program was planned to screen a large number of alloys on the basis of rupture resistance alone, select a few alloys for further evaluation, and then choose one alloy for fuller characterization.

Thirty-six alloys were chosen to consider the response of the Ni-Al-Mo system to alloy modification. Additions of Ta, Ta+Cr, V, V+Cr, Re, Re+Cr, V+Re, V+W, Ta+Ti, Re+Ti, and Ta+V+Re+Ti were considered. Of this group, 7 alloys were superior to AG-60 in rupture at 850°C, 12 alloys at 1100°C, and 4 alloys at both conditions.

Based on these results, 3 of the alloys plus 3 new alloys were chosen for further evaluation. The most potent strengthening element in the first 36 alloys was V; therefore, all 6 alloys contained at least 2 atom percent V, and one contained 4 atom percent V. Other concepts pursued in this further evaluation included V+W, V+Re, V+Ta+Re+Ti and V+Ta+Re+Ti+Cr. These alloys were tested in longitudinal and transverse tension and in longitudinal rupture, with and without prior cyclic temperature exposure. The most heavily alloyed material could not be fully aligned at a solidification rate of 1 cm/h. Three of the alloys were nearly equivalent (V, V+Re, and V+Ta+Re+Ti) in terms of a balance of the measured behavior.

Alloy 38 (AG-170) was given the most extensive evaluation. This alloy contains by weight percent, 5.88 Al, 29.74 Mo, 1.65 V and 1.20 Re, and the balance Ni. It presents no major problem in solidification. Its demonstrated solidification rate (1 cm/h) at blade processing temperature gradients is somewhat less than for AG-60, but greater than for either NiTaC-13 or γ/γ'-δ. No reactivity of the liquid alloy with 3 different mold materials was observed. The alloy is processible to hollow blade shapes using currently available mold and core ceramics.

Alloy 38 has greater longitudinal tensile strength at high temperatures than most conventional superalloys, but is weaker than the directionally solidified eutectics NiTaC**-13 and γ/γ'-δ over most of the temperature

*AG is a General Electric Corporate Research and Development alloy designation.

**NiTaC is a generic designation for nickel based eutectic alloys reinforced with monocarbide whiskers.

range. In the transverse direction, its tensile strength equals that of AG-60 and NiTaC-13, while its elongation shares with that of AG-60 a significant advantage over that of other eutectic systems. The tensile shear strength of alloy 38 is intermediate between AG-60 and NiTaC-13 and substantially better than γ/γ'-δ.

The stress rupture strength of alloy 38 in the longitudinal direction was generally greater than AG-60 at low stress, high-temperature rupture conditions; and its low-temperature rupture strength could be improved beyond that of AG-60 by the proper choice of the coating process cycle. The alloy in the coated plus coating heat-treated condition is more resistant to stress rupture than the base AG-60 at all stresses. It is also within 1 Larson-Miller (T = 1.8 K) parameter of NiTaC-13 at 800 MPa, and is 2 parameters above NiTaC-13 at 100 MPa. In transverse stress rupture, uncoated alloy 38 is comparable to AG-60, providing a significant strength advantage over other eutectics at high stresses. Cyclic and isothermal exposure up to 1000 hours at 750°C prior to testing at that temperature appeared to have no effect on the rupture strength. However, exposure up to 1000 hours at 1100°C decreased the rupture life between one-third and one-half; a comparable exposure of NiTaC-13 produces a rupture life decrease by two-thirds. Since in actual blade service only a small fraction of the design life is spent at 1100°C for any portion of the turbine blade, the observed degradation is small. Compared to conventional superalloys exposed to 1000°C, alloy 38 cycled to 1100°C offers improved stability to rupture life loss during service exposure.

Dynamic modulus behavior was similar to current aircraft blade alloys, but the thermal expansion coefficients were significantly smaller than for current alloys. This may be beneficial in reducing thermal strains resulting from temperature gradients in turbine airfoils. At the same time, the low expansion behavior may require different coating compositional concepts to achieve a compatible alloy/coating system. The alloy may need a coating on the internal cooling passage surfaces as well as on the outer blade surface to prevent excessive oxidation.

Based on the results obtained in this program, alloy 38 (AG-170) represents an improvement beyond alloy AG-60. Both of these alloys, as well as possibly others in the γ/γ'-α (Mo) eutectic system, may be considered as potential alternate or superior blade materials to those of the NiTaC and γ/γ'-δ eutectic systems.

Section 2

INTRODUCTION

Throughout its entire history, advances in turbine blade materials technology have been fundamental to the evolution of the jet engine. The continuous need for better materials has resulted in an increase in metal capability of 5^{o} to 10^{o}C per year. Since the 1950's, growth has depended on new gamma-prime-strengthened nickel superalloys which, in turn, have required the development of vacuum processes for melting the increasingly complex alloys. Further improvements have been made through directional solidification. Directionally solidified alloys have better rupture and thermal fatigue lives because of the virtual elimination of weakening grain boundaries normal to the major stress axis and the low elastic modulus of the grains along the major stress axis. Because ductility is increased in directionally solidified superalloys, they have been heavily alloyed to increase their strength, while maintaining adequate ductility for blade applications. However, it now appears that further dramatic advances in directionally solidified superalloys cannot be readily achieved.

Better turbine blade materials are being sought in many laboratories through various approaches, including: synthesized composites using strong filamentary reinforcements, directional eutectics (in situ composites), oxide-dispersion-strengthened alloys, single crystals, and ceramics. Of these, the most promising candidates are judged by General Electric to be the directional eutectics. In the early 1960's, it was recognized that directional solidification of eutectics was a feasible method for producing composites. Although aligned eutectic composites lacked the flexibility in reinforcement/matrix combinations of the synthesized composites, they offered solutions to many of the problems confronting the latter type in high-temperature applications. Specifically, eutectic composites offered two major potential advantages: 1) high-temperature chemical compatibility of phases and 2) fabrication simplification. There was also the possibility of whisker-like, high strength in one phase from crystal perfection and the desired strong bond between the phases through interphase diffusion at the solidification temperature. These materials are far along the path for use in engines.

The successful use of eutectics in jet-engine, high-pressure turbine blade applications requires the development of many new or improved technologies, including:

- Development of an alloy to meet some preset property goals
- Development of internal and external coatings for the higher eutectic blade temperature capability
- Early assessment of eutectic blade manufacture and demonstration of performance in component bench and engine tests

- Establishment of a cost-effective manufacturing method for casting complex, cooled, high-pressure turbine blades
- Demonstration of eutectic, high-pressure turbine blade performance in bench and engine tests
- Development of industry capability (including involvement of vendors) to manufacture cost-effective eutectic blades
- Acquisition of design data and development of design practices

For the NiTaC eutectic systems, such a full evaluation has been underway at General Electric for a number of years. However, another eutectic system, γ/γ'-αMo, is receiving attention as a blade material. This system was identified in a recent NASA-sponsored program [ref. 1] which had as its objective the production of at least one new directionally solidified eutectic alloy from among 6 systems studied for potential use in jet aircraft engine turbine blades. The property goals (Table I) for the new alloy were superior to those of the eutectic alloys already undergoing extensive study. These goals were, at least in part, met by the γ/γ'-αMo system. A developmental program of other γ/γ'-αMo eutectics is being performed under NAVAIR sponsorship [refs. 2 through 5] in addition to the present program.

TABLE I. - PROPERTY GOALS FOR EUTECTIC ALLOY DEVELOPMENT

1.	Longitudinal tensile strength at 750°C of 1050 MN/m^2 (150 000 psi) and at 1100°C of 700 MN/m^2 (100 000 psi)
2.	Elongation of at least 5 percent in longitudinal tensile tests at all temperatures
3.	A 1000-hour longitudinal rupture life at 750°C under 700 MN/m^2 (100 000 psi) stress and at 1100°C under 140 MN/m^2 (20 000 psi) stress
4.	Ability to withstand 500 hours (at 1 cycle/h) of cycling between 425°C or less and 1150°C with less than a 10 percent decrease in stress rupture resistance
5.	Longitudinal shear strength of not less than 35 percent of the longitudinal tensile strength
6.	Oxidation resistance equal to that of Hastelloy-X at 750°C and 1100°C
7.	Aligned structure when solidified at a rate of 2 cm/h or greater for a thermal gradient of 100°C/cm or less with a 1.25-cm-diameter bar
8.	A melting point of not less than 1250°C
9.	A density of not over 9.15 g/cm^3 (0.330 lb/in^3)
10.	A transverse tensile elongation of $>$ 1 percent at room temperature

Work in the literature on the Ni-Al-Mo eutectic was very limited prior to the NASA program. Thompson and Lemkey [ref. 6] reported on a Ni_3Al-Mo eutectic with 26 v/o fibers, a melting point of 1306°C, a density of 8.18 gm/cm^3, a Young's modulus of 138 GN/m^2 (19.7x10^6 psi) and room-temperature tensile properties of 1120 MN/m^2 (160 ksi), ultimate strength with 21 percent elongation. The composition reported by Ashbrook [ref. 7] was Ni-8 w/o Al -27 w/o Mo. Henry [ref. 8] later showed that there is no γ'-α eutectic in the Ni-Al-Mo system. Rather, the alloys solidify as γ-α, with subsequent precipitation of γ' from the γ matrix. For sufficiently high Al contents, the γ can be completely consumed by γ' precipitation.

In contract NAS3-19711 [ref. 1], the alloy AG-60, Ni-13.2 a/o (5.7 w/o) Al and 21 a/o (32.3 w/o) Mo, was found to have an excellent balance of strength and ductility. The exceptional properties of this alloy make it an excellent choice to serve as a base composition for development of an alloy for aircraft turbine blade applications. The microstructure consists of regular and continuous rods of αMo in a matrix of a Ni-rich γ that contains the Ni_3Al γ' phase as precipitates. The strength properties of the alloy are in the same range as the more mature eutectics, NiTaC-13 and γ/γ'-δ. The density of the material is 8.65 g/cm^3. Directional solidification at 2 cm/h results in a well aligned structure; higher rates may be possible. An advantage of the γ/γ'-αMo eutectic system over these other eutectics is the good ductility of both the matrix and the reinforcement. The solidification temperature of the AG-60 alloy is approximately 1300°C. The cyclic oxidation resistance of the simple three-element Ni-Al-Mo alloys is essentially equivalent to NiTaC-13 and γ/γ'-δ, indicating that coatings will be critical to the use of this alloy as a blade material; the system is more processable than either NiTaC-13 or γ/γ'-δ. Mold systems based on Al_2O_3/SiO_2 will probably be adequate, but cores other than SiO_2 will be needed.

To evaluate the γ/γ'-αMo system, a number of properties must be characterized, since turbine blade design encompasses a wide spectrum of material properties. The airfoil operates in a very high-temperature environment under both centrifugal stress and stresses generated by the gas loads, the temperature distribution, and the pressure fluctuations. The modulus of elasticity determines the thermal stress and the blade natural frequencies; the coefficient of expansion contributes to both the thermal stress levels and the blade growth; the thermal conductivity affects the thermal gradients and the transient airfoil temperature profiles. The combined centrifugal, thermal, and gas bending stresses can be evaluated on a modified Goodman diagram to find the airfoil life limit due to stress rupture and high cycle fatigue. Other potential sources of airfoil failure include thermal fatigue, oxidative metal loss or alloy depletion, hot corrosion, foreign object damage, and creep instability due to unusual overtemperature conditions.

Attachment of the blade to the disk requires a different approach in design and in required material properties. A single or multiple tang dovetail supports the entire centrifugal load of the airfoil, the platform and the shank, transmitting the blade loads to the supporting disk at the tang pressure faces. The operating temperature of the attachment area is usually kept below 650°C in order to take maximum advantage of the disk material yield strength. Ductility and low cycle fatigue capability are critical in dovetail design. The blade material must be able to yield locally and redistribute the load so that an averaging effect of the working stress level is achieved after the first few cycles. Without good ductility, notch sensitivity would be higher and overall cyclic life would be less.

A special consideration for eutectics is the directionality of the properties. Both longitudinal and transverse mechanical/physical properties are required to fully engineer the alloy and the design into a solid working package.

The purpose of the present program was to improve — through changes in composition — the γ/γ'-αMo alloy, AG-60, previously identified in contract NAS3-19711. Since the scope of the properties important to blade design is too large to evaluate for a number of alloys, the program was planned to screen a large number of alloys on the basis of rupture resistance alone, select a few alloys for further evaluation, and then choose one alloy for fuller characterization.

In the first task, 36 alloys were evaluated microstructurally at two growth rates, and their aligned structures were tested in stress rupture at 850°C and 1100°C. For improved stress rupture resistance over the range of turbine blade service temperatures, the simple ternary γ/γ'-α system offers compositional flexibility to influence the γ, γ', and α phases separately or in combination. For the γ phase, the elements W, Re, and V are known to provide strengthening by solid solution hardening. The elements Ta and Ti, as well as V, are potent in strengthening Ni_3Al. For Mo, all of these elements exhibit appreciable to complete solid solubility; some, such as Ta, increase the lattice parameter of Mo; and others, such as V, decrease the lattice parameter. Additions of Cr can also be considered for improved oxidation resistance. The partitioning of Cr will be predominantly in the γ and α phases.

Based on the rupture behavior of these alloys, 6 compositions were chosen for evaluation in Task II. Again, structural evaluations were performed, and the alloys were tested in rupture at 750°C and 1100°C. Bars were also thermally cycled to 1100°C for 150 hours and rupture tested at 1100°C. The tensile strength and ductility of each alloy was evaluated at 750°C and 1100°C in both the longitudinal and transverse orientations.

Finally, a single alloy was chosen for testing in Task III. This involved: microstructural evaluation; creep rupture at 750°C and 1100°C; stress rupture at 750°C, 850°C, 950°C, and 1100°C; transverse stress rupture at 750°C and 950°C; thermal cycling to 1100°C followed by rupture at 750°C and 1100°C; 1000 hours exposure at 750°C and 1100°C followed by rupture at the exposure temperature; tensile tests at 23°C, 600°C, 750°C, 850°C, 950°C, and 1100°C; transverse tensile tests at 750°C and 950°C; and longitudinal shear tests at 750°C and 1100°C. A number of coated specimens were tested in rupture at 750°C, 950°C, and 1100°C; and in tension at 23°C, 600°C, 750°C, 950°C, and 1100°C. Uncoated specimens were heat treated to simulate the coating cycle and then ruptured at 750°C and 1100°C. The incipient melting temperature was also determined for the coated alloy. Dynamic modulus and coefficient of thermal expansion were determined, and the cyclic oxidation behavior of the alloy at 750°C and 1100°C was measured. The reactivity of the liquid alloy was measured in three mold materials and two core materials.

Section 3

MATERIALS AND PROCEDURES

MELTING

Raw metal charges were melted in alumina crucibles in an argon atmosphere using a motor-generator induction heater at approximately 10 kHz. Elements such as Al were added after initial melting. The melts were superheated about 300°C, cooled to measure a thermal arrest temperature, remelted, and poured into copper chill molds. Typical material purities were:

Element	Maximum total impurities percent	Major nonvolatile impurity
Al	0.01	60 ppm Si
Cr	0.5	0.35% Fe
Mo	0.3	0.04% Fe
Ni	0.02	0.01% C
Re	0.02	100 ppm W
Ta	0.02	40 ppm W
Ti	0.3	0.03% Fe
V	0.2	0.15% Si
W	0.5	0.05% Mo, Si

DIRECTIONAL SOLIDIFICATION

Directional solidification was performed in modified Bridgman furnaces. The smaller ingots were directionally solidified by in situ melting 2-cm-diameter melt stock in 2-cm-diameter recrystallized Al_2O_3 crucibles in an argon atmosphere. The furnace had a graphite susceptor that was inductively heated by a radio frequency (approximately 450 kHz) induction power supply. The ingot sat on a water-cooled copper side chill during directional solidification; temperature gradients were approximately 100°C/cm. The smaller 2-cm-diameter ingots were generally 9- to 11-cm long.

The larger ingots were produced by melting the alloy master melt in an upper melting chamber with a motor-generator set and pouring the molten

charge into 4-cm-diameter recrystallized Al_2O_3 crucibles. The heat source in this apparatus was a resistance-heated, wire-wound furnace tube; temperature gradients were approximately 130°C/cm. Turbine blade shapes were directionally solidified in this same apparatus.

STRUCTURE EVALUATION AND SECTIONING

Initial evaluation of the structure of the directionally solidified ingots in all of the tasks was performed by grinding a longitudinal flat along the entire length of the ingot and polishing it to a metallographic finish for microscopic examination as-polished. The Task-I ingots were then documented for lengths of chill-cast structure, hyper- or hypoeutectic structure, aligned structure, and/or cellular structure. From this evaluation, the ingot was scheduled for machining into test specimens or a modification was performed on the chemistry or solidification rate. The ingot sectioning schedules used in Task I are shown in Figure 1. The cut between pieces Nos. 2 and 3 was selected to be approximately 1.25 cm above the top of the sort-out zone, if present. Piece No. 3 was used as test bars. Piece Nos. 2 and 4 were checked for density, and the top of piece No. 2 and the bottom of piece No. 4 were polished for transverse microstructural evaluation.

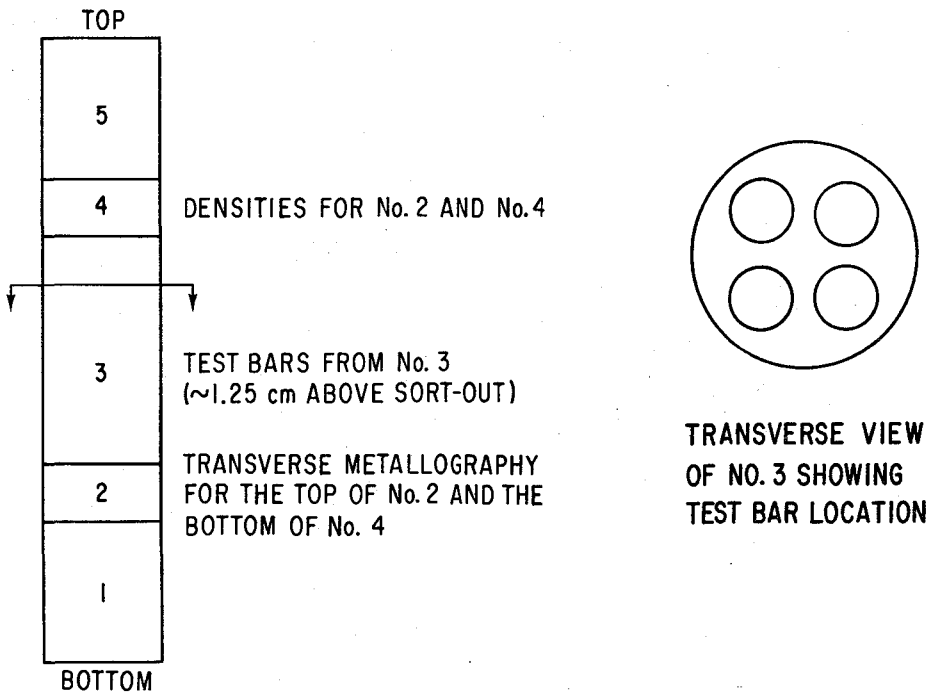

Figure 1. - Schematic Sectioning Diagram for Directionally Solidified Ingots.

Alloys in the γ/γ'-αMo system exhibit a wide range of microstructures. Visual standards set for the transverse cross sections were used for all of the tasks, while those set for the longitudinal cross sections were used in Tasks II and III.

Visual standards were set for classification of the structures from longitudinal views, for Task-II and -III alloys, in a fashion analogous to the transverse standards reported. On the longitudinal sections, it was extremely difficult to distinguish between those structures rated as 4 and 5 on the transverse. Therefore, the visual standards for longitudinal classification were:

Longitudinal rating	Corresponding transverse rating
A	1
B	2
C	3
D	4 and 5

Visual standards used for classification of the longitudinal sections are shown in Figure 2.

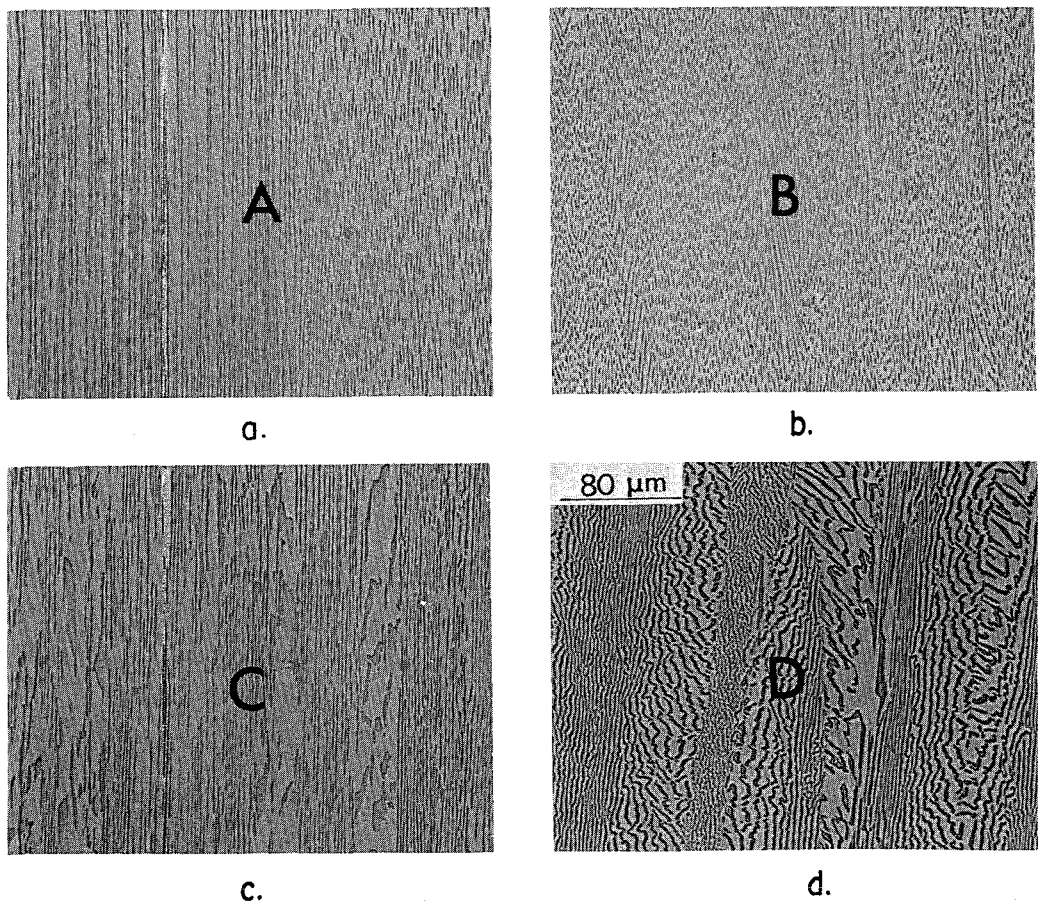

Figure 2. - Visual Standards for Degree of Alignment in γ/γ'-αMo Longitudinal Sections. a) Rating = A, b) Rating = B, c) Rating = C, d) Rating = D.

Visual standards used for classification of the transverse sections of the ingots scheduled for testing are shown in Figure 3. The structures are rated as 1 through 5 in progression from aligned to cellular:

Rating	Classification
1	Aligned; possibly some plates at grain boundaries
2	Bimodal distribution of fiber sizes in a nonsymmetric cell-like pattern
3	Incipient cells with a breakdown to plates at the cell boundaries
4	Large, irregular cells
5	Small, symmetric cells

For directional castings (4-cm diameter) from Tasks II and III, microstructures on the polished longitudinal flats were classified according to the longitudinal visual standards. Transverse classifications were more reliable because of the presence of a rim or edge effect for some compositions. Rims of structure different from the bulk of the ingot center were observed to vary in thickness from composition to composition. In no case did the gauge of a mechanical test specimen contain any microstructure not typical of the bulk of the ingot. A 5.2-cm length was then cut from the Task-II ingots for longitudinal and transverse mechanical test specimens. The ends of this 5.2-cm section were metallographically polished, and the structure at each end was classified according to the transverse visual standards. For the Task-III ingots, two sections were cut for specimens. A 4.2-cm length was taken from the bottom of each ingot for creep longitudinal rupture, thermal expansion, dynamic modulus and cyclic oxidation specimens. A section either 4.2 cm or 5.2 cm in length was taken from the top for longitudinal and transverse tensile, transverse rupture, creep, thermal expansion, and longitudinal shear test specimens. Sections from the bottom and the top of the ingots were taken for transverse microstructure classification and fluorescence chemical analysis.

DENSITY DETERMINATION

Densities were determined on coupons from the aligned sections of the directionally solidified ingots. The density was calculated from weights of the coupons in air and in glycol.

TENSILE TESTS

The specimen design used for the longitudinal and transverse tensile tests is shown in Figure 4. The specimens were tested in split grips in a screw-driven Instron tensile machine. The specimens were tested in air at room temperature, and in a capsule at approximately a 5-μm Hg pressure vacuum level at other temperatures. The crosshead rate used was 0.5

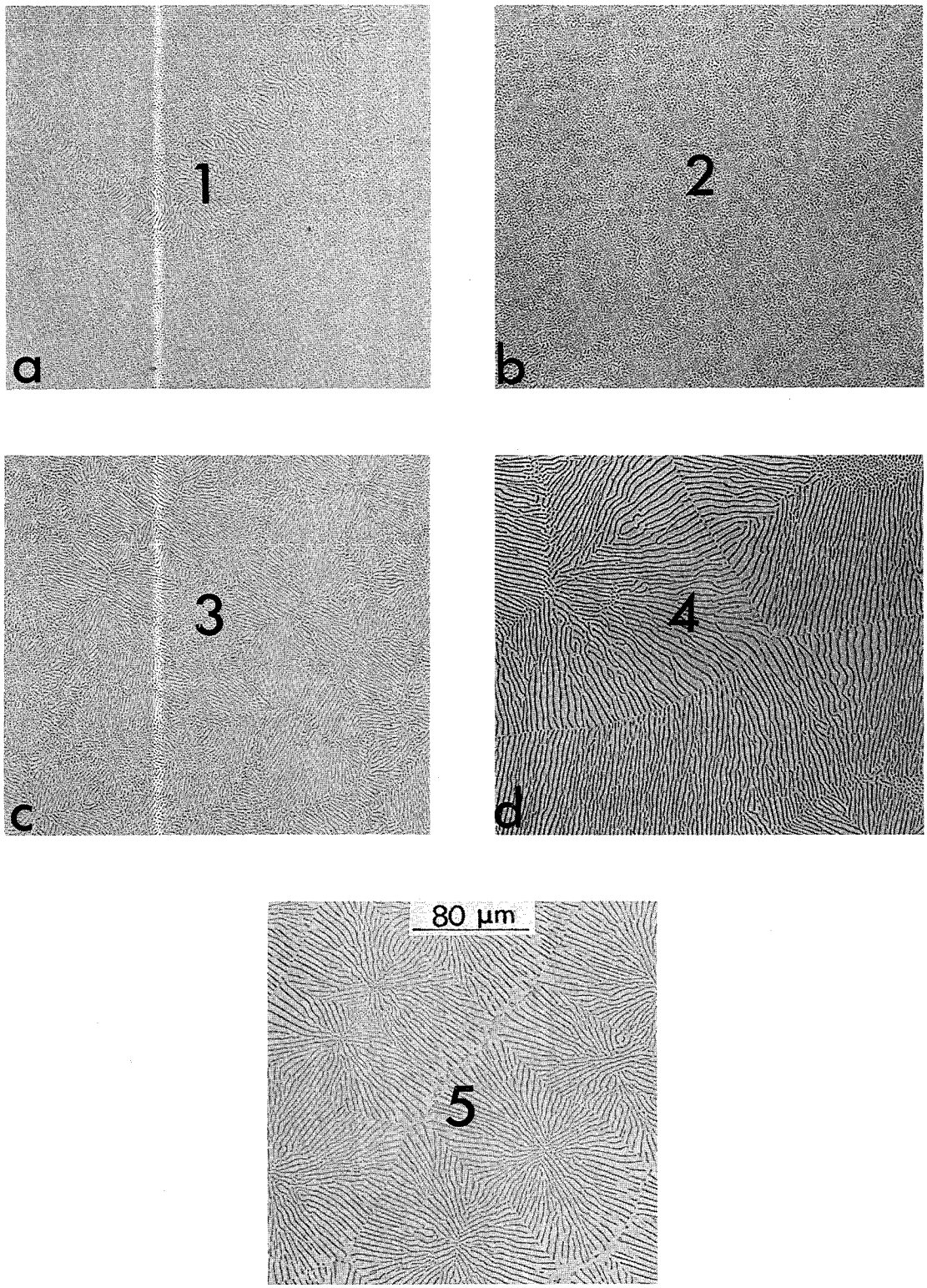

Figure 3. - Visual Standards for Degree of Alignment in γ/γ'-αMo Transverse Sections. a) Rating = 1, b) Rating = 2, c) Rating = 3, d) Rating = 4, e) Rating = 5.

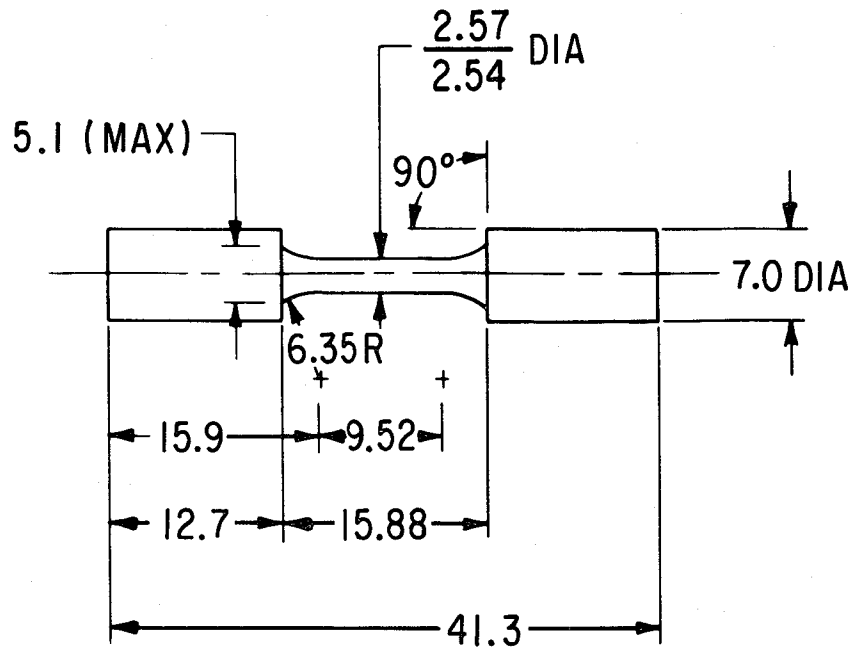

DIMENSIONS IN mm
TENSILE AND RUPTURE SPECIMEN

Figure 4. - Specimen Used for Tensile and Creep Rupture Tests.

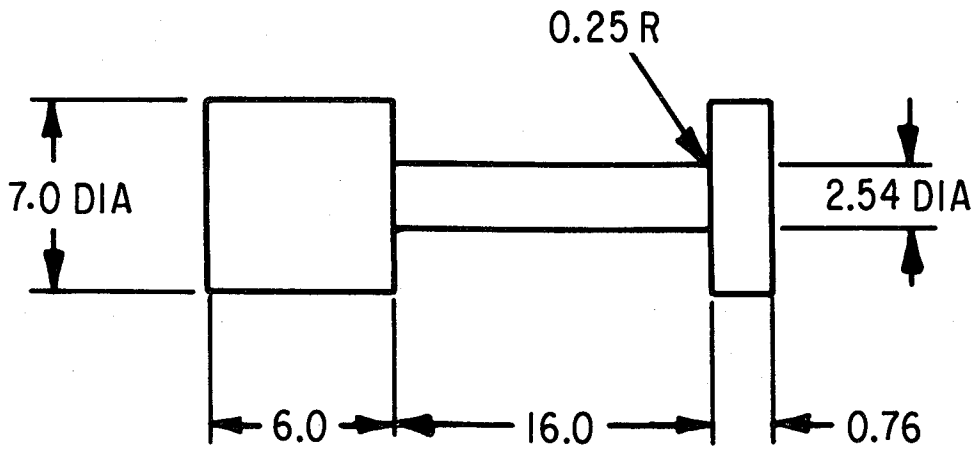

DIMENSIONS IN mm
LONGITUDINAL SHEAR SPECIMEN

Figure 5. - Specimen Used for Longitudinal Shear Tests.

cm/min. The effective gauge length was taken as 1.14 cm, yielding a plastic strain rate of 0.044 min^{-1}. Load vs. time was recorded, from which was extracted 0.2 percent yield strength, ultimate tensile strength, strain-to-maximum load, and strain to failure. Reduction in area was measured on each test bar.

LONGITUDINAL SHEAR TESTS

For longitudinal shear strength, a specimen was designed with a shear area equal to the minimum area perpendicular to the principal stress. The specimen design is shown in Figure 5. The specimen consisted of a uniform section having a diameter of 0.41 cm and a one-button head 0.10 cm in length. The shear area is then π x 0.41 x 0.10 or approximately 0.13 cm^2. The specimens were tested in split grips at a crosshead rate of 0.05 cm/min, and the load vs. time was recorded.

This test, while not a pure shear test, was a good evaluation of the in-service loading conditions.

CREEP AND STRESS RUPTURE TESTS

The specimen design used for the longitudinal and transverse stress rupture and longitudinal creep tests was the same as that used for the tensile tests (see Figure 4). The tests were run as constant load tests in 135 kPa (abs) argon. Specimen elongation was monitored in the creep tests to determine time to 0.02, 0.05, 0.2, 0.5, and 1 percent creep strain.

THERMAL CYCLING AND ISOTHERMAL EXPOSURES

Specimen blanks 0.7 cm in diameter by 4.4 cm in length were used for the thermal cycling and isothermal exposures. The specimen blanks were cycled or exposed isothermally in evacuated quartz tubes in a static air, resistance-wound furnace tube. Isothermal treatments were at 750°C and 1100°C. The thermal cycle consisted of a one-hour period, with 50 minutes in the furnace and 10 minutes outside the furnace, which was automated for continuous operation. A thermocouple recorded the temperature on a strip-chart recorder. The specimens cooled to approximately 200°C and spent approximately 45 minutes at the furnace temperature of 1100°C during each cycle. The furnace temperature was maintained through the use of a thermocouple and a continuously monitoring proportional controller.

After thermal cycling or isothermal exposure, a short piece was cut off the end of each blank for metallographic examination. The remainder was machined into a stress rupture specimen.

CYCLIC OXIDATION

The apparatus and cycle used for the static air, cyclic oxidation tests were the same as those used for the thermal cycling. The test specimens were 0.25 cm in diameter by 4-cm in length. Maximum temperatures of 1100°C, 1000°C, and 750°C were used, as designated. Periodic weight change measurements were made.

CERAMIC/METAL REACTIVITY

A ceramic/metal reactivity test was performed to evaluate the reactivity of the candidate shell mold and core materials for directional solidification of turbine blades. The blade castings were grown with a superheat of approximately 250°C in a Bridgman apparatus having an upper pouring chamber. Reactivity was determined by metallographic examination.

THERMAL EXPANSION

Bars 0.64 cm in diameter and 4.2 cm in length were used to determine the coefficients of linear thermal expansion on heating and cooling between room temperature and 1100°C. A standard SiO_2 bar was used for continuous differential length measurements as the furnace was heated at a rate of 5°C/min and cooled at a rate of 5°C/min. Tests were performed in the laboratories of Theta, Inc., Port Washington, New York.

DYNAMIC MODULUS

Bars 0.25 cm in diameter and 4.2 cm in length were used to determine the dynamic modulus. The specimens were welded to a Ni-W alloy rod and placed in a resistance-wound furnace in an argon atmosphere. An ultrasonic pulse was initiated in the specimen and the echo pulse frequency was matched to a signal of known frequency, f. Knowing the specimen length, ℓ, and density, ρ, the modulus was calculated from $E = K\rho\,(\ell f)^2$, where K was a dimensional constant. Determinations were made at 25°C and at 100°C intervals on heating to and cooling from 1225°C.

FLUORESCENCE CHEMICAL ANALYSIS

Intensities of characteristic x-ray lines for Ni, Al, Mo, V, and Re generated with a Cr x-ray tube were measured on several Task-III ingot chill-cast sections and an aligned region. Data were collected using 2.2-cm-diameter masks, and three separate runs were performed to check repeatability. An arithmetic average of the characteristic intensities for three chill-cast sections was made for each element; these averages were then used to calculate the chemical compositions, assuming the average characteristic intensities were representative of the nominal Task-III alloy

composition. The calculation was made using Cicciarelli's "QUAN" program [ref. 9].

COATING

Standard test bars (Figure 4) and 0.25-cm-diameter pins of the Task-III alloy were grit blasted and coated with IN-671 (Ni-50 Cr with a small volume fraction of TiC) powder in a low-pressure/high-velocity plasma-spray system. Coatings of 75 to 100-μm thickness were deposited on only the gauge length for the test bars and over the entire surface for the pins. The pins were used to determine, by metallographic observation, incipient melting conditions for the coated, Task-III alloy after one-hour exposures at several temperatures. Based on these observations, the coated test bars were heat treated for one hour at 1260°C (+0, -5°C) to accomplish diffusion bonding.

Section 4

RESULTS

PRELIMINARY EVALUATION OF ALLOY CONCEPTS

In Task I of this program, 36 alloys were selected for evaluation and approved by the NASA Project Manager. These alloys examined several concepts for additions to the simple Ni-Al-Mo system. The following concepts were examined:

System		Alloys
Ni-Al-Mo	+ Ta	(1-4)
	+ Ta + Cr	(5-6)
	+ V	(7-15)
	+ V + Cr	(16-17)
	+ Re	(18-23)
	+ Re + Cr	(24-25)
	+ V + Re	(26-27)
	+ V + W	(28-29)
	+ Ta + Ti	(30-31)
	+ Re + Ti	(32-33)
	+ Ta + V + Re + Ti	(34-36)

The chemistries of these Task-I alloys are given in Tables II and III.

Structure of Task I Alloys

Each alloy was directionally solidified at 2 cm/h and 1 cm/h in a thermal gradient of approximately 100°C/cm. A test plan was formulated to perform stress rupture testing in argon at 850°C/485 MPa and at 1100°C/110 MPa for all of the 1 cm/h bars, those bars at 2 cm/h which exhibited aligned structure, and some selected nonaligned 2 cm/h bars. Evaluation of the longitudinal microstructures of the Task-I alloys and the transverse microstructures of those alloys scheduled for test are listed in Table IV. The average measured density of the aligned structures and the thermal arrest temperatures for the nominal melt chemistries are also listed. The total range for the arrest temperature is only 31°C, and there is little evidence for a systematic variation in the arrest temperature with composition, except for a slight tendency for increased temperature with increased Al

TABLE II. - COMPOSITION OF TASK-I ALLOYS IN ATOMIC PERCENT

Alloy	AG No.	Ni	Al	Mo	Ta	V	Re	W	Ti	Cr
-	60	65.8	13.2	21.0						
1	105	64.5	13.0	21.5	1.0					
2	106	64.5	11.0	23.5	1.0					
3	108	64.5	12.0	21.5	2.0					
4	109	64.5	10.0	23.5	2.0					
5	107	62.5	13.0	20.5	1.0					3.0
6	110	62.5	10.0	22.5	2.0					3.0
7	111	64.5	12.0	21.5		2.0				
8	112	64.5	10.0	23.5		2.0				
9	114	64.5	10.0	21.5		4.0				
10	115	64.5	8.0	23.5		4.0				
11	130	63.75	10.0	22.25		4.0				
12	131	63.75	8.0	24.25		4.0				
13	132	64.0	12.0	21.0		3.0				
14	133	64.0	11.0	22.0		3.0				
15	134	64.0	9.0	24.0		3.0				
16	113	62.5	12.0	20.5		2.0				3.0
16A	113A	62.0	12.0	21.0		2.0				3.0
17	116	62.5	8.0	22.5		4.0				3.0
18	117	64.9	14.0	20.7			0.4			
19	118	64.9	12.0	22.7			0.4			
20	120	65.3	13.0	20.9			0.8			
21	121	65.3	11.0	22.9			0.8			
22	135	64.9	12.0	22.5			0.6			
23	136	64.9	14.0	20.5			0.6			
24	119	62.9	14.0	19.7			0.4			3.0
25	122	63.3	11.0	21.9			0.8			3.0
26	123	64.9	12.5	20.2		2.0	0.4			
27	124	64.9	11.0	21.7		2.0	0.4			
28	125	64.9	12.5	20.2		2.0		0.4		
29	126	64.9	11.0	21.7		2.0		0.4		
30	127	65.0	12.0	21.0	1.0				1.0	
31	128	65.0	10.0	23.0	1.0				1.0	
32	140	65.2	11.0	22.4			0.4		1.0	
33	141	65.2	13.0	20.4			0.4		1.0	
34	137	64.55	9.0	23.15	0.5	2.0	0.3		0.5	
35	138	64.55	11.0	21.15	0.5	2.0	0.3		0.5	
36	139	64.55	13.0	19.15	0.5	2.0	0.3		0.5	

TABLE III. - COMPOSITION OF TASK-I ALLOYS IN WEIGHT PERCENT

Alloy	AG No.	Ni	Al	Mo	Ta	V	Re	W	Ti	Cr
-	60	62.0	5.7	32.3						
1	105	59.3	5.5	32.3	2.9					
2	106	58.0	4.6	34.6	2.8					
3	108	57.9	5.0	31.6	5.5					
4	109	56.8	4.0	33.8	5.4					
5	107	58.0	5.6	31.1	2.8					2.5
6	110	55.5	4.1	32.6	5.4					2.4
7	111	60.3	5.2	32.9		1.6				
8	112	59.0	4.2	35.2		1.6				
9	114	59.9	4.3	32.6		3.2				
10	115	58.6	3.3	34.9		3.2				
11	130	58.9	4.3	33.6		3.2				
12	131	57.7	3.3	35.9		3.1				
13	132	60.1	5.2	32.2		2.5				
14	133	59.5	4.7	33.4		2.4				
15	134	58.2	3.8	35.6		2.4				
16	113	59.0	5.2	31.7		1.6				2.5
16A	113A	58.4	5.2	32.3		1.6				2.5
17	116	57.3	3.4	33.7		3.2				2.4
18	117	61.0	6.0	31.8			1.2			
19	118	59.6	5.1	34.1			1.2			
20	120	60.5	5.5	31.6			2.4			
21	121	59.2	4.6	33.9			2.3			
22	135	59.5	5.1	33.7			1.7			
23	136	60.8	6.0	31.4			1.8			
24	119	59.7	6.1	30.5			1.2			2.5
25	122	57.9	4.6	32.8			2.3			2.4
26	123	60.9	5.4	30.9		1.6	1.2			
27	124	59.8	4.7	32.7		1.6	1.2			
28	125	60.9	5.4	30.9		1.6		1.2		
29	126	59.9	4.6	32.7		1.6		1.2		
30	127	59.8	5.1	31.5	2.8				0.8	
31	128	58.5	4.1	33.8	2.8				0.8	
32	140	59.8	4.6	33.6			1.2		0.8	
33	141	61.2	5.6	31.2			1.2		0.8	
34	137	57.2	3.7	34.1	1.4	2.3	0.9		0.4	
35	138	58.5	4.6	31.8	1.4	2.4	0.9		0.4	
36	139	59.8	5.6	29.4	1.4	2.5	0.9		0.4	

TABLE IV. - STRUCTURES OF TASK-I ALLOYS

Alloy	AG No.	T_{freeze} (°C)	Density (g/cm^3)	DS No.	DS rate (cm/hr)	Longitudinal structure*	Transverse structure** (2T†)	Transverse structure** (4B†)
1	105	1297	8.80	2867	2	7 mm CC/9 mm FSO/114 mm C	1	1
1	105	1297	8.78	2950	1	10 mm CC/20 mm FSO/32 mm IC/45 mm C	S + 1	S + 1, 2
2	106	1287	--	2862	2	10 mm CC/1 mm FSO/126 mm C	--	--
2	106	1287	8.96	2915	1	12 mm CC/4 mm FSO/64 mm IC/56 mm C	1	1 - 4
3	108	1297	8.97	2866	2	9 mm CC/13 mm FSO/110 mm C	2	2,3
3	108	1297	8.95	2922	1	11 mm CC/14 mm FSO/107 mm C	S + 1,2	2
4	109	1291	--	2869	2	9 mm CC/7 mm FSO/104 mm C	--	--
4	109	1291	9.08	2952	1	8 mm CC/11 mm FSO/121 mm C	S + 1	1
5	107	1292	--	2864	2	7 mm CC/12 mm FSO/115 mm C	--	--
5	107	1292	8.73	2920	1	8 mm CC/16 mm FSO/55 mm A/37 mm C	S + 1	1
6	110	1291	--	2870	2	12 mm CC/18 mm FSO/104 mm C	--	--
6	110	1291	9.0	2925	1	15 mm CC/26 mm FSO/85 mm C	S + 3	4
7	111	1292	8.67	2871	2	10 mm CC/3 mm FSO/70 mm A/40 mm C	1,2	1,2
7	111	1292	8.67	2926	1	5 mm CC/6 mm FSO/15 mm IC/35 mm A/60 mm IC	1	1
8	112	1292	8.83	2873	1.8	10 mm CC/2 mm FSO/113 mm C	1	1
8	112	1292	8.82	2827	1	16 mm CC/1 mm FSO/8 mm C/45 mm A/60 mm C	1	1
9	114	1282	8.76	2877	2.3	13 mm CC/<1 mm FSO/8 mm IC/101 mm C	1	1,2
9	114	1282	8.75	2934	1	7 mm CC/<1 mm FSO/90 mm A/30 mm C	1	1
10	115	1297	--	2879	1.8	9 mm CC/<1 mm FSO/8 mm C/102 mm MD	--	--
10	115	1297	8.91	2936	1	6 mm CC/<1 mm MSO 26 mm C/46 mm IC/38 mm C	1	1
11	130	1307	8.70	2993	2	13 mm CC/6 mm FSO/12 mm IC + S/50 mm A/30 mm C	1	1,2
11	130	1307	8.73	2995	1	7 mm CC/11 mm FSO/78 mm A/29 mm C	1	1
12	131	1299	8.89	3007	2	10 mm CC/3 mm FSO/97 mm C/19 mm MD	3,4	3,4
12	131	1299	8.89	3023	1	10 mm CC/5 mm FSO/51 mm IC/79 mm C	1	1
13	132	1302	8.65	3011	2	11 mm CC/5 mm FSO/23 mm IC + S/28 mm IC/75 mm C	1,2	1,2
13	132	1302	8.83	3025	1	14 mm CC/6 mm FSO/70 mm A/52 mm C	1	1
14	133	1300	8.71	3013	2	14 mm CC/3 mm FSO/4 mm C + S/110 mm C/7 mm MD	3	3,4
14	133	1300	8.71	3027	1	15 mm CC/5 mm FSO/35 mm A/35 mm C	1	1
15	134	1300	--	3015	2	1 mm CC/<1 mm FSO/20 mm IC/75 mm C/25 mm MD	--	--
15	134	1300	8.84	3029	1	12 mm CC/1 mm FSO/10 mm C/40 mm A/65 mm C	1	1
16	113	1287	8.61	2918	2	11 mm CC/4 mm FSO/42 mm IC/80 mm C	1	3
16	113	1287	8.64	2931	1	8 mm CC/2 mm FSO/43 mm A/62 mm C	1	1
16A	113A	1296	--	2902	2	7 mm CC/8 mm FSO/122 mm C	--	--
16A	113A	1296	8.60	2930	1	11 mm CC/16 mm FSO/75 mm A/24 mm C	1	1,3
17	116	1292	8.82	2881	2.23	12 mm CC/<1 mm FSO/115 mm C	4,5	2,4
17	116	1292	8.81	2938	1	10 mm CC/<1 mm FSO/10 mm C/18 mm IC/74 mm C/3 mm MD	1,2	3,4
18	117	1303	8.62	2888	2	12 mm CC/6 mm FSO/17 mm IC/41 mm A/55 mm C	3,4	5
18	117	1303	8.64	2941	1	11 mm C/16 mm FSO/17 mm IC/80 mm A/15 mm C	1	1
19	118	1300	8.82	2890	2	7 mm CC/2 mm FSO/35 mm IC/83 mm C/2 mm MD	3	5
19	118	1300	8.81	2944	1	11 mm CC/3 mm FSO/10 mm IC/75 mm A/20 mm IC/20 mm	1	1
20	120	1295	8.80	2896	2	10 mm CC/6 mm FSO/120 mm C	5	5
20	120	1295	8.77	2954	1	9 mm CC/8 mm FSO/14 mm IC/19 mm A/70 mm IC	1,4	1
21	121	1296	--	2898	2	9 mm CC/<1 mm FSO/75 mm C/37 mm FD/1 mm MD	--	--
21	121	1296	8.91	2978	1	12 mm CC/<1 mm FSO/13 mm C/26 mm IC/85 mm C	1	1
22	135	1304	--	3016	2	10 mm CC/0 mm FSO/109 mm C/10 mm MD	--	--
22	135	1304	8.85	3031	1	13 mm CC/3 mm FSO/63 mm A/57 mm C	1	1
23	136	1313	--	3017	2	14 mm CC/7 mm FSO/116 mm C	--	--
23	136	1313	8.87	3033	1	13 mm CC/7 mm FSO/10 mm IC + S/80 mm A/30 mm C	1	1
24	119	1287	--	2894	2	9 mm CC/10 mm FSO/100 mm C	--	--
24	119	1287	8.55	2947	1	11 mm CC/30 mm FSO/66 mm A/26 mm C	1	1
25	122	1288	--	2900	2	10 mm CC/<1 mm FSO/130 mm C	--	--
25	122	1288	8.85	2960	1	9 mm CC/7 mm FSO/89 mm IC	1	5
26	123	1303	8.70	2904	2	12 mm CC/1 mm FSO/116 mm C	4,5	5
26	123	1303	8.69	2962	1	6 mm CC/3 mm FSO/14 mm C/35 mm IC/65 mm C	1,4	1
27	124	1308	8.84	2906	2	9 mm CC/<1 mm FSO/41 mm C/65 mm FD + MD	1,3	5
27	124	1308	8.84	2964	1	5 mm CC/2 mm MD/3 mm C/13 mm IC/34 mm A/22 mm IC/25 mm C	1	1
28	125	1302	8.70	2910	2	10 mm CC/2 mm FSO/55 mm IC/65 mm C	1,2	3,4
28	125	1302	8.68	2968	1	10 mm CC/5 mm FSO/7 mm C/65 mm A/50 mm C	1	1
29	126	1305	8.80	2911	2	8 mm CC/1 mm FSO/120 mm C/6 mm FD + MD	5	5
29	126	1305	8.79	2970	1	10 mm CC/<1 mm FSO/10 mm C/<1 mm FSO/17 mm IC/97 mm C	1	1
30	127	1301	8.80	2912	2	9 mm CC/26 mm FSO/91 mm C	1	1,4
30	127	1301	8.83	2972	1	8 mm CC/22 mm FSO/65 mm Ic	1	2
31	128	1286	8.92	2916	2	8 mm CC/2.5 mm FSO/115 mm C	4	4
31	128	1287	8.95	2990	1	14 mm CC/6 mm FSO/6 mm C/44 mm IC/38 mm C	1	1
32	140	1300	--	3019	2	15 mm CC/1 mm FSO/5 mm IC/115 mm C	--	--
32	140	1300	8.97	3037	1	10 mm CC/6 mm FSO/64 mm A/28 mm C	1	1
33	141	1304	--	3021	2	7 mm CC/6 mm FSO/92 mm C	--	--
33	141	1304	8.71	3039	1	12 mm CC/7 mm FSO/32 mm A/54 mm C	1	3
34	137	1298	--	3096	2	15 mm CC/1 mm FSO/113 mm C	--	--
34	137	1298	8.89	3071	1	12 mm CC/3 mm FSO/55 mm A+C/41 mm C	1	1
35	138	1306	--	3098	2	13 mm CC/9 mm FSO/107 mm C	--	--
35	138	1306	8.83	3077	1	10 mm CC/8 mm FSO/52 mm A+C/30 mm C	1	1
36	139	1304	--	3100	2	12 mm CC/28 mm FSO/79 mm C	--	--
36	139	1304	8.62	3083	1	8 mm CC/28 mm FSO/58 mm A/31 mm C	1,2	1

*CC Chill cast
FSO Mo sort-out
MSO Matrix sort-out
A Aligned
IC Incipient cellular
C Cellular
FD Mo dendritic
MD Matrix dendritic
S Mo star-like particles

**Structures classified as in Figure 3, plus S = Mo star-like particles.

†Metallography on top of Section 2, bottom of Section 4 in Figure 1.

content. The densities are essentially proportional to the density calculated by assuming atom fraction contributions on an elemental density basis.

Most of the alloys showed good alignment at 1 cm/h, but many could not be fully aligned over any length at 2 cm/h. Structural alignment tended to decrease as Al was decreased or as Cr was added. Of the three single element additions, V had the least detrimental effect on alignment, and Re and Ta were about equivalent in reducing alignment, on an atomic percent addition basis.

Longitudinal classifications of a flat ground on an ingot are not as reliable as transverse classifications for interpretation of mechanical specimen data, because the ingots sometimes exhibited an outer rim where, as determined in the transverse view, the structure was different than in the center of the 22-mm diameter cross section. These rims ranged from very shallow, 0.02 mm (0.001 inch), to very deep, 2.5 mm (0.1 inch). The depth of the longitudinal stripes measured on several randomly selected ingots ranged from 0.20 mm (0.008 inch) to 0.58 mm (0.023 inch), with an average value of 0.33 mm (0.013 inch). For those ingots with a rim effect, the longitudinal stripe could penetrate or lie completely within the rim. However, for the current specimen design, the gauge section material could never be closer than 2.5 mm (0.1 inch) to the edge.

Stress Rupture Properties of Task-I Alloys

Results of rupture testing at 850°C and 1100°C are given in Table V. Since several nonaligned ingots were tested intentionally, the data are presented graphically in Figure 6 together with information on alloy chemistry and ingot microstructure. A poorly aligned structure tends to result in shorter lives, especially at the high test temperature.

A comparison of the Task-I alloys against AG-60 is shown in Table VI. This scorecard is quite impressive. Improvements in rupture life due to chemistry modifications were obtained at 850°C in 64 percent of the alloys, at 1100°C in 47 percent of the alloys, and at both temperatures in 31 percent of the alloys.

From the table and the figure, it appears that additions of 1 to 2 a/o Ta or Ta + Ti to the γ/γ'-αMo system generally lower rupture resistance at 1100°C, and increase it at 850°C; additions of 3 a/o Cr to any of the alloys tends to be very slightly detrimental; Ti added to Re-containing alloys has a possible neutral/negative effect. The most potent alloy addition, singly or in combination with other elements, was V. For rupture at both 850°C and 1100°C, V was the only element that was consistently beneficial. Additions of Re were beneficial at 1100°C, but had little effect at 850°C.

TABLE V. - STRESS RUPTURE RESULTS ON TASK-I ALLOYS

(In argon atmosphere)

Alloy	AG No.	DS rate (cm/h)	Stress rupture 850°C/485 MPa			Stress rupture 1100°C/110 MPa		
			Life (h)	Elongation (%)	R.A. (%)	Life (h)	Elongation (%)	R.A. (%)
--	60	2	102	--	--	155	--	--
--	60	1	43	--	--	131	--	--
1	105	2	90	25	33	145	33	70
1	105	1	54	30	45	158	27	68
2	106	1	48	33	52	92	23	77
3	108	2	40	31	53	34	29	24
3	108	1	29	25	40	25	23	35
4	109	1	91	23	50	87	22	75
5	107	1	67	31	47	67	31	47
6	110	1	69	32	58	42	19	73
7	111	2	246	28	43	228	22	64
7	111	1	65	32	54	162	18	44
8	112	2	112	20	44	75	27	76
8	112	1	37	34	47	70	13	41
9	114	2	189	24	31	100	18	47
9	114	1	68	21	32	73	26	80
10	115	1	27	18	21	45	26	84
11	130	2	100	22	40	154	20	69
11	130	1	61	32	39	134	12	62
12	131	1	33	27	32	36	31	61
13	132	2	132	29	45	178	12	28
13	132	1	74	32	44	134	20	65
14	133	1	59	30	40	139	20	66
15	134	1	51	20	40	51	20	75
16	113	2	120	30	50	169	11	36
16	113	1	57	31	54	167	17	64
16A	113A	1	81	36	57	153	10	41
17	116	2	43	34	43	13	20	76
17	116	1	24	33	61	12	9	19
18	117	2	16	42	65	233	21	68
18	117	1	9	42	68	250	20	80
19	118	2	247	31	54	112	13	41
19	118	1	51	45	66	147	13	59
20	120	2	29	26	43	15	27	37
20	120	1	31	37	65	196	11	51
21	121	1	26	13	57	5	13	69
22	135	1	46	34	68	149	19	68
23	136	1	37	13	22	229	25	75
24	119	1	25	39	67	186	22	62
25	122	1	36	43	72	64	22	60
26	123	2	40	37	41	21	14	47
26	123	1	66	32	58	219	12	58
27	124	2	12	20	36	3	30	80
27	124	1	73	30	54	117	17	71
28	125	2	109	22	37	170	16	45
28	125	1	55	32	53	219	14	64
29	126	2	11	25	47	3	34	71
29	126	1	56	39	49	178	13	58
30	127	2	93	18	24	145	24	53
30	127	1	79	16	23	24	4	6
31	128	2	24	29	46	6	26	73
31	128	1	60	27	48	102	24	81
32	140	1	37	38	63	82	22	77
33	141	1	49	27	28	120	20	48
34	137	1	51	31	36	43	20	80
35	138	1	70	24	42	128	23	69
36	139	1	17	31	60	317	23	68

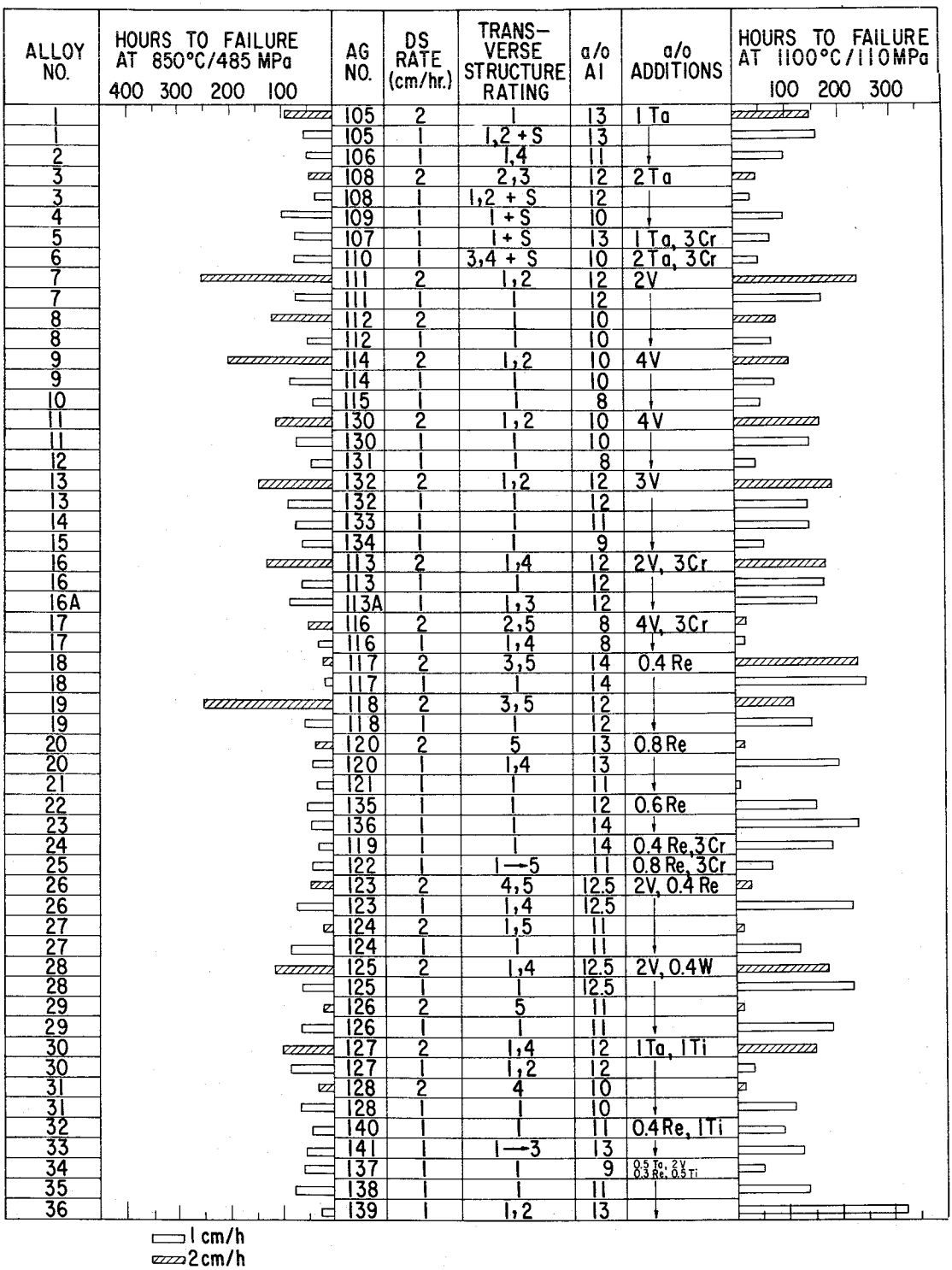

Figure 6. - Bar Chart of Task-I Stress Rupture Lives.

TABLE VI. - COMPARISON OF 36 TASK-I ALLOYS AND BASE ALLOY AG-60 IN STRESS RUPTURE RESISTANCE IN VACUUM

	Number of Alloys
Comparing alloys grown at 1 cm/h with AG-60 grown at 1 cm/h:	
Alloys with improved 850°C resistance	23
Alloys with improved 1100°C resistance	17
Alloys with improved resistance at both	11
Comparing alloys grown at 2 cm/h with AG-60 grown at 2 cm/h:	
Alloys with improved 850°C resistance	7
Alloys with improved 1100°C resistance	5
Alloys with improved resistance at both	4
Comparing alloys grown at 1 or 2 cm/h with AG-60 grown at 2 cm/h:	
Alloys with improved 850°C resistance	7
Alloys with improved 1100°C resistance	12
Alloys with improved resistance at both	4

REFINEMENT OF ALLOY CONCEPTS

The results of the Task-I testing were used to select 6 compositions for inclusion in Task II. Three of these were Task-I alloys, and three were modifications of the Task-I alloys. The selected alloys and their growth rates are listed in Table VII. The growth rates were chosen based on the Task-I structural evaluation. Alloy 37 was grown at both 1 and 2 cm/h in order to enable evaluation of the growth rate effect in this alloy.

Of the alloying concepts listed in section "Preliminary Evaluation of Alloy Concepts" (page 19), the most promising were V, Re, V + Re, V + W, and Ta + V + Re + W. The addition of Re alone did not offer low-temperature rupture resistance, consequently that concept was abandoned. For the V concept, two alloys were chosen: alloy 7, the best balanced alloy from Task I; and a new alloy 37, with 4 V at a higher Al content than was considered in Task I, combining the features of alloys 11 and 13. For the V + Re concept, a new alloy 38 was chosen; it is based on alloy 26, but with added Al. For the V + W concept, alloy 28 was chosen. For the Ta + V + Re + W concept, alloy 36 was chosen. This alloy had the highest measured lifetime in 1100°C stress-rupture. The 850°C rupture life was surprisingly low, based on the contents of Ta, Ti, and V and the effects of those elements in the other alloys. To further evaluate the concept of a complex multielement

TABLE VII. - TASK-II ALLOY COMPOSITIONS AND GROWTH RATES

Alloy	AG No.	Ni	Al	Mo	Ta	V	Re	W	Ti	Cr	Growth rate cm/h
					Atomic Percent						
7	111	64.5	12	21.5		2					2
28	125	64.9	12.5	20.2		2		0.4			1
36	139	64.55	13	19.15	0.5	2	0.3		0.5		1
37	142	64.0	12	20.0		4					1, 2
38	170	64.9	13.5	19.2		2	0.4				1
39	171	62.55	13	18.15	0.5	2	0.3		0.5	3	1
					Weight Percent						
7	111	60.3	5.2	32.9		1.6					2
28	125	60.9	5.4	31.0		1.6		1.2			1
36	139	59.8	5.6	29.4	1.4	1.6	0.9		0.4		1
37	142	60.6	5.2	30.9		3.3					2
38	170	61.6	5.9	29.7		1.6	1.2				1
39	171	59.3	5.7	28.1	1.5	1.6	0.9		0.4	2.5	1

γ/γ'-αMo alloy, a variation was made to alloy 36 by adding 3 a/o Cr; alloy 36 then became alloy 39.

As noted in Table VI, four alloys showed net gains over the best AG-60 properties at both 850°C and 1100°C. Alloys 7 and 28 were carried into Task II, and alloy 13 was modified to the new alloy 37. Only alloy 16, similar to alloy 7 but containing Cr, was not pursued further.

Structure of Task-II Alloys

Results of the longitudinal and transverse metallographic examinations are listed in Table VIII. Since the bottom cut of DS No. LDB*-289 was made at the transition from "C" structure to "A-B" structure on the longitudinal stripe, the transverse rating on that plane is probably worse than and not representative of the structure slightly further up the ingot.

The first ingot attempted for alloy 7 (DS No. LB*-302 at 2 cm/h) had an anomalous solidification behavior. Transverse sectioning revealed the presence of a large, irregular-shaped region near the center of the bar with

*LB and LDB are General Electric Corporate Research and Development ingot number designations for 4-cm-diameter ingots.

TABLE VIII. - STRUCTURE OF TASK-II INGOTS

(4-cm diameter)

Alloy	AG No.	Rate (cm/h)	DS No.	T_{freeze} (°C)	Total length (cm)	Chill-cast length (cm)	Mo sort-out length (cm)	Longitudinal structure rating*	Transverse structure rating** of 5.2-cm section	
									Bottom	Top
7	111	2	LDB-303	1304	16.8	2.3	0.1	11.0 cm A/B, 3.4 cm C/D	2	2
28	125	1	LDB-296	1310	17.5	2.2	0.1	1 cm C, 13.2 cm A, 1 cm C	1-2	1-2
36	139	1	LDB-297	1303	15.5	1.8	2.4	7.6 cm A + S, 3.7 cm C/D	1-S	1-3
37	142	1	LDB-289	1305	17.8	0.9	0.5	2 cm C, 10.2 cm A/B, 4.2 cm D	3-4	1-2
37	142	2	LDB-300	1303	18.0	2.0	0.2	12.7 cm A, 3.1 cm D	2	2
38	170	1	LDB-298	1310	19.0	2.3	0.3	15.3 cm A, 1.1 cm C/D	1	1
39	171	1	LDB-299	1299	18.2	2.4	3.5	9.1 cm A/C, 3.2 cm D	3-S	4-5

*See Figures 2 and 3 for classification.
**S = Mo star-like particles.

cellular structure. The structure outside that region, on the same transverse plane, was essentially aligned. This ingot then had sufficient thermal gradient to give aligned structure, but simultaneously had aligned and non-aligned structure growing. This is different from the "rim effect" reported previously. Work sponsored by NAVAIR has noted similar effects in other γ/γ'-α Mo alloys, where the structure has been named a "cat's eye" [ref. 5]. This seems to be a new type of growth defect not previously observed in other eutectics.

Figures 7 and 8 show typical structures from aligned and cellular ingots, respectively. Figure 7 shows the typical structure from alloy 38 grown at 1 cm/h (DS No. LDB-298) which was classified as aligned. Figure 8 shows the typical structure from alloy 39 grown at 1 cm/h (DS No. LDB-299), which was classified as cellular.

Tensile Properties of Task-II Alloys

Two longitudinal and two transverse tensile tests were performed for each alloy, one each at 750°C and 1100°C in vacuum at a nominal strain rate of 0.044 min^{-1}. The results are given in Table IX for the 750°C tests and in Table X for the 1100°C tests.

The 750°C tensile results are excellent. The 750°C longitudinal tensile strengths range from 0.94 to 1.09 of the tensile strength goal established under NASA contract NAS 3-19711 for this temperature. The 750°C transverse tensile strengths are excellent and range from 0.89 to 0.98 of the longitudinal value. The 750°C transverse minimum percent elongation to failure was 5.0, far better than the NiTaC-13 or γ/γ'-δ eutectics.

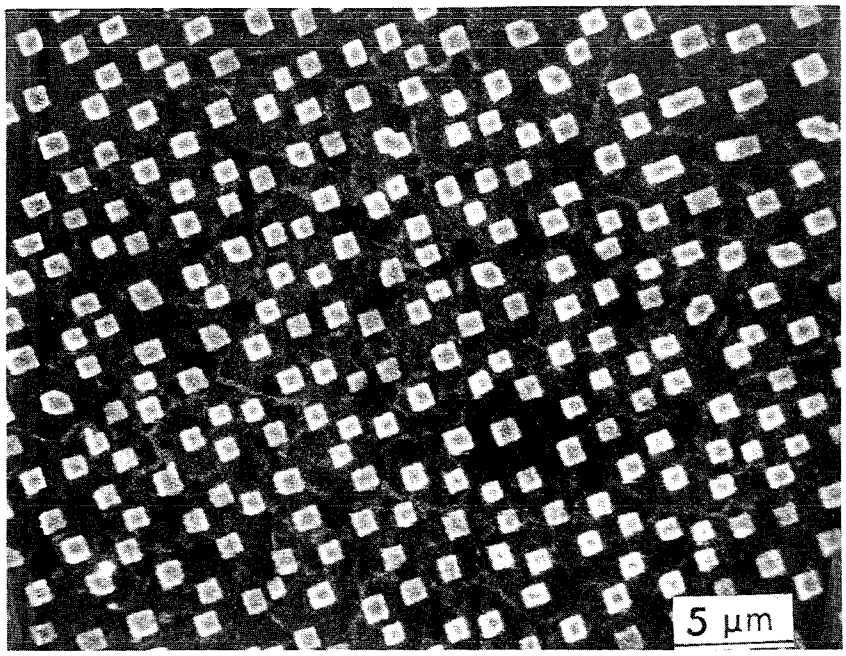

Figure 7. - Photomicrograph of Transverse Section of DS No. LDB-298 (Alloy 38) at 1 cm/h.

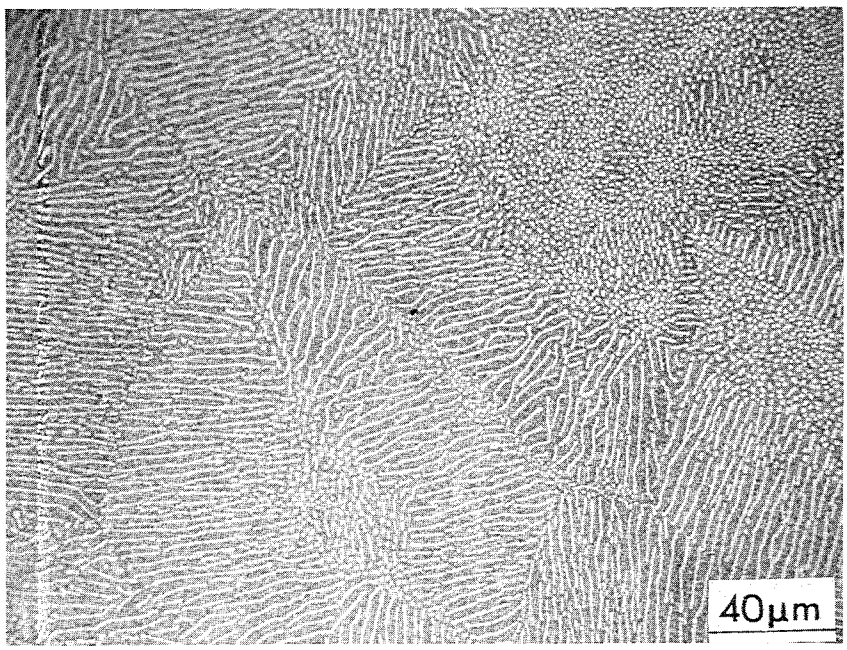

Figure 8. - Photomicrograph of Transverse Section of DS No. LDB-299 (Alloy 39) at 1 cm/h.

TABLE IX. - TASK-II TENSILE RESULTS AT 750°C (0.044 $min.^{-1}$ in vacuum)

Alloy	AG No.	DS rate (cm/h)	0.2% offset yield strength (MPa)	Ultimate tensile strength (MPa)	Elongation to maximum load (%)	Elongation to failure (%)	R.A. (%)
			Longitudinal				
--	60	2	965-986	1083-1110	--	15-18	27-34
7	111	2	979	1089	9.5	29	35
28	125	1	938	1041	9.1	22	36
36	139	1	931	1007	7.3	19	40
37	142	2	1041	1145	15.0	40	40
37	142	1	924	1014	6.8	16	36
38	170	1	910	986	9.9	18	34
39	171	1	979	1034	5.1	15	52
			Transverse				
--	60	2	889	924	--	5.4	17
7	111	2	903	986	5.8	6.2	16
28	125	1	883	938	6.7	8.0	26
36	139	1	752	938	9.5	9.5	12
37	142	2	917	1020	4.4	6.4	14
37	142	1	889	993	9.3	12.0	13
38	170	1	848	896	5.0	5.0	20
39	171	1	821	934	6.4	8.4	18

TABLE X. - TASK-II TENSILE RESULTS AT 1100°C (0.044 $min.^{-1}$ in vacuum)

Alloy	AG No.	DS rate (cm/h)	0.2% offset yield strength (MPa)	Ultimate tensile strength (MPa)	Elongation to maximum load (%)	Elongation to failure (%)	R.A. (%)
			Longitudinal				
--	60	2	432-449	441-457	--	40-41	87
7	111	2	396	427	0.9	50	83
28	125	1	343	364	1.0	60	97
36	139	1	427	444	0.9	60	92
37	142	2	452	467	0.7	56	75
37	142	1	365	391	1.0	54	97
38	170	1	418	430	0.8	57	82
39	171	1	408	421	0.8	41	84
			Transverse				
--	60	2	266	281	--	61	≃80
7	111	2	250	267	0.7	33	75
28	125	1	280	296	0.8	28	22
36	139	1	296	311	1.1	52	99
37	142	2	285	303	0.7	23	9.3
37	142	1	276	289	0.8	15	13
38	170	1	312	325	0.7	16	6
39	171	1	188	208	1.2	41	85

The 1100°C tensile results show that the Task-II alloys are very similar to AG-60 in terms of both strength and ductility. For all of the Task-II alloys except one, the 1100°C transverse strengths range from 0.63 to 0.81 of the longitudinal strengths; for AG-60 this value is about 0.63. The one alloy showing anomalous behavior is alloy 39, which has a transverse/longitudinal strength ratio of 0.49. Alloy 39 was the ingot with cellular microstructure. In all cases, the transverse ductility is far in excess of the goal of NASA contract NAS 3-19711. For both longitudinal and transverse orientations, alloy 37 was slightly stronger for the 2 cm/h structure, both at 750°C and 1100°C.

Stress Rupture Properties of Task-II Alloys

For the Task-II alloys, the stress-rupture test conditions selected were 750°C/775 MPa (1382°F/112.4 ksi) and 1100°C/125 MPa (212°F/18.1 ksi). For alloys 7, 28, and 36 these tests complement the Task-I stress rupture testing at 850°C/485 MPa (1562°F/70.3 ksi) and 1100°C/110 MPa (2012°F/16.0 ksi). The Task-II stress-rupture results are given in Table XI. A smooth curve drawn through the data for the base alloy, AG-60, at 2 cm/h was used to calculate the lives for the Task-II rupture conditions. Only alloy 7 is superior to AG-60 at the 750°C test condition. However, for the 1100°C test condition, both alloys 7 and 37 grown at 2 cm/h are better than AG-60. For the alloys grown at 1 cm/h, three of the five alloys show longer rupture lives than 2 cm/h AG-60. Alloy 37 was stronger at 750°C in the 2 cm/h structure, compared to the 1 cm/h structure. There was no difference in the 1100°C rupture testing.

Thermal Cyclical Effects on Stress Rupture Properties of Task-II Alloys

For each of the Task-II alloys, longitudinal slugs previously cycled 150 hours between 200°C and 1100°C were machined into stress-rupture specimens. The results of rupture testing at 1100°C/125 MPa are listed in Table XII. All of the alloys except alloy 28 showed a decrease in rupture life after cycling. The alloy with cellular microstructure (alloy 39) showed the largest decrease, losing 79 percent of the as-solidified rupture life. Alloys 36, 37 (2 cm/h and 1 cm/h) and 38 are roughly equivalent in rupture life in the as-cycled condition. Of these three, alloy 36 showed the greatest loss after cycling, and alloy 38 the least. Alloy 28 showed a marked increase in life after cycling, but it is believed that the as-directionally solidified life is anomalously low. A comparison with the Task-I 1100°C rupture test suggests a longer life is expected.

In an attempt to determine if a correlation exists between microstructural changes and rupture strength degradation, each of the Task-II alloys was examined metallographically after thermal cycling. Comparisons of typical microstructures as directionally solidified and after 150 cycles to 1100°C are shown in Figure 9 for alloy 36 and in Figure 10 for alloy 28.

TABLE XI. - TASK-II STRESS RUPTURE RESULTS

(In argon atmosphere)

Alloy	AG No.	DS rate (cm/h)	750°C/775 MPa			1100°C/125 MPa		
			Life (h)	Elongation (%)	R.A. (%)	Life (h)	Elongation (%)	R.A. (%)
--	60*	2	130	--	--	50	--	--
7	111	2	140	20	39	62	23	64
28	125	1	84	20	50	31	29	86
36	139	1	51	22	46	175	39	86
37	142	2	89	25	32	128	23	61
37	142	1	26	20	33	123	21	59
38	170	1	52	23	37	116	28	74
39	171	1	34	24	39	43	16	58

*Lives calculated from rupture curve.

TABLE XII. - TASK-II THERMAL CYCLING RESULTS

(Cycled in evacuated quartz tubes)

Alloy	AG No.	DS rate (cm/h)	1100°C/125 MPa			t_{cycled}/t_{virgin}
			Life (h)	Elongation (%)	R.A. (%)	
7	111	2	28	18	47	0.45
28	125	1	70	37	69	2.26
36	139	1	118	47	78	0.67
37	142	2	88	27	65	0.69
37	142	1	92	31	84	0.75
38	170	1	106	35	78	0.91
39	171	1	9	20	71	0.21

Note: All specimens cycled 150 times at one hour per cycle between 1100°C and less than 300°C prior to stress-rupture testing.

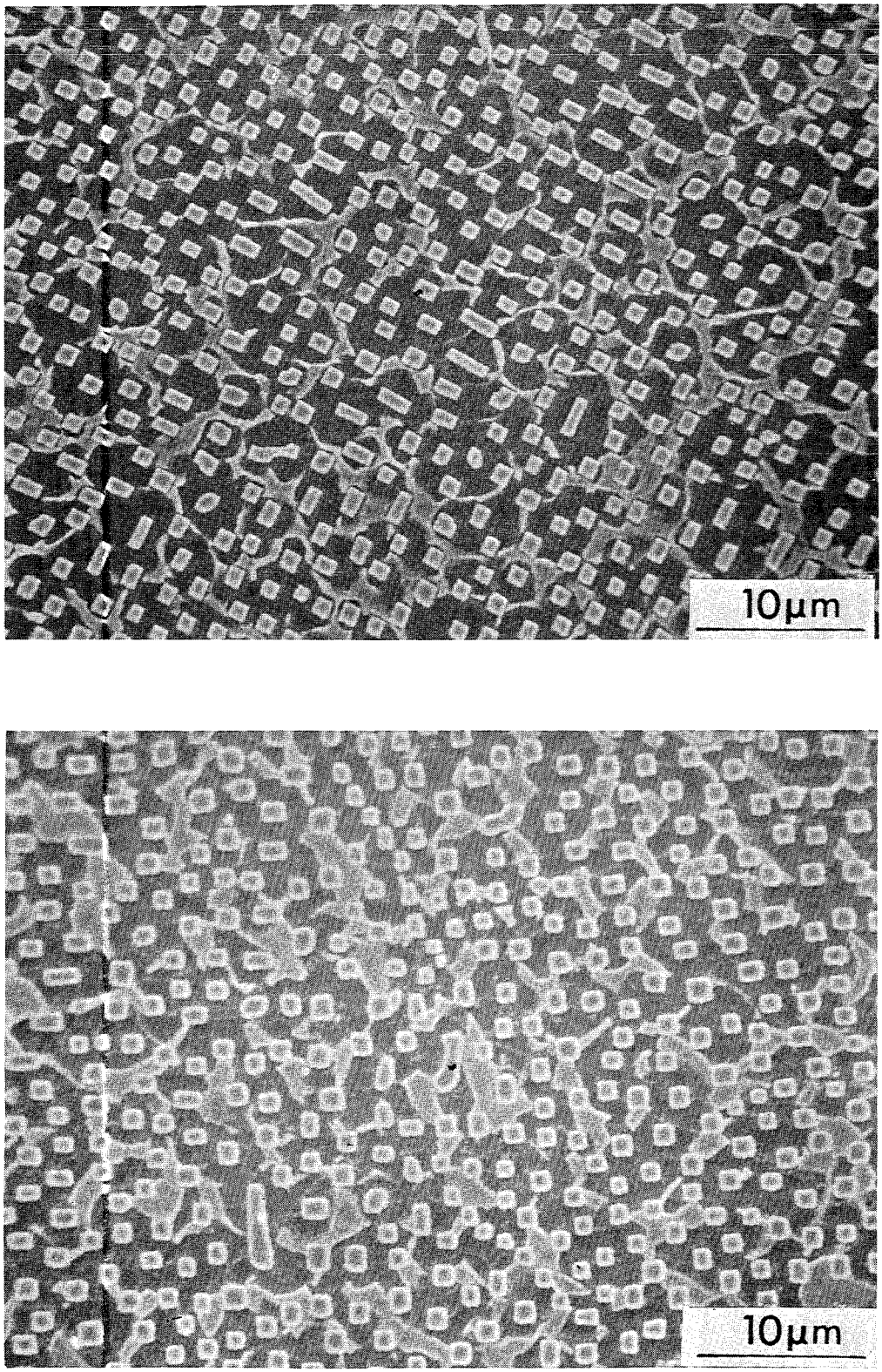

Figure 9. - Transverse Microstructure of Alloy 36:
a) As Directionally Solidified
b) After 150 Thermal Cycles to 1100°C.

a

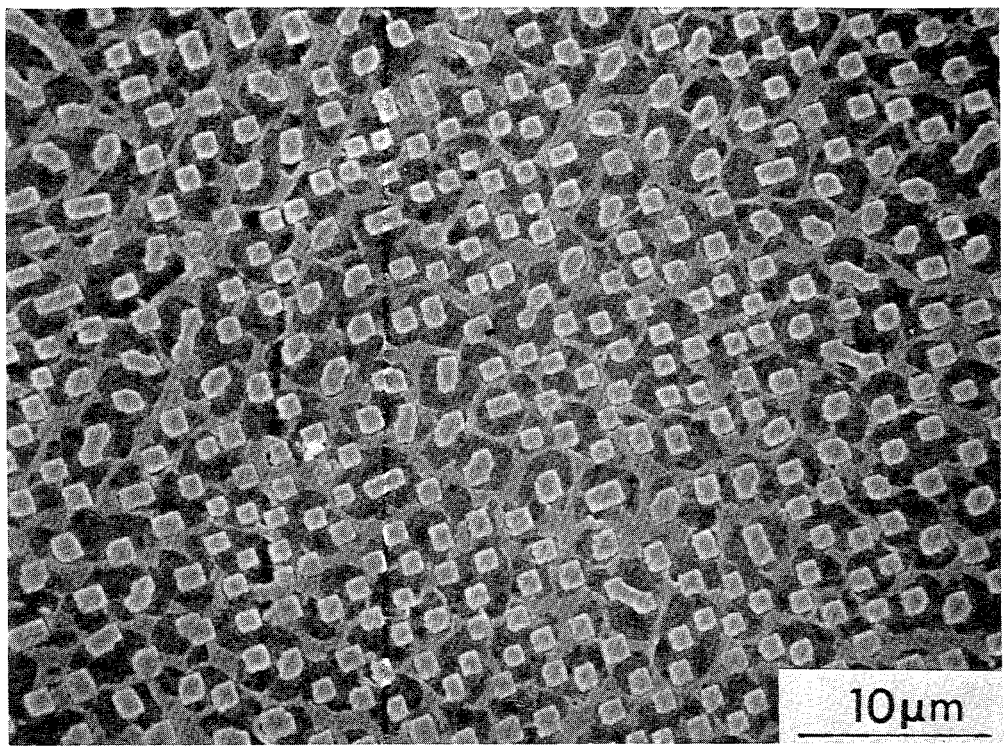

b

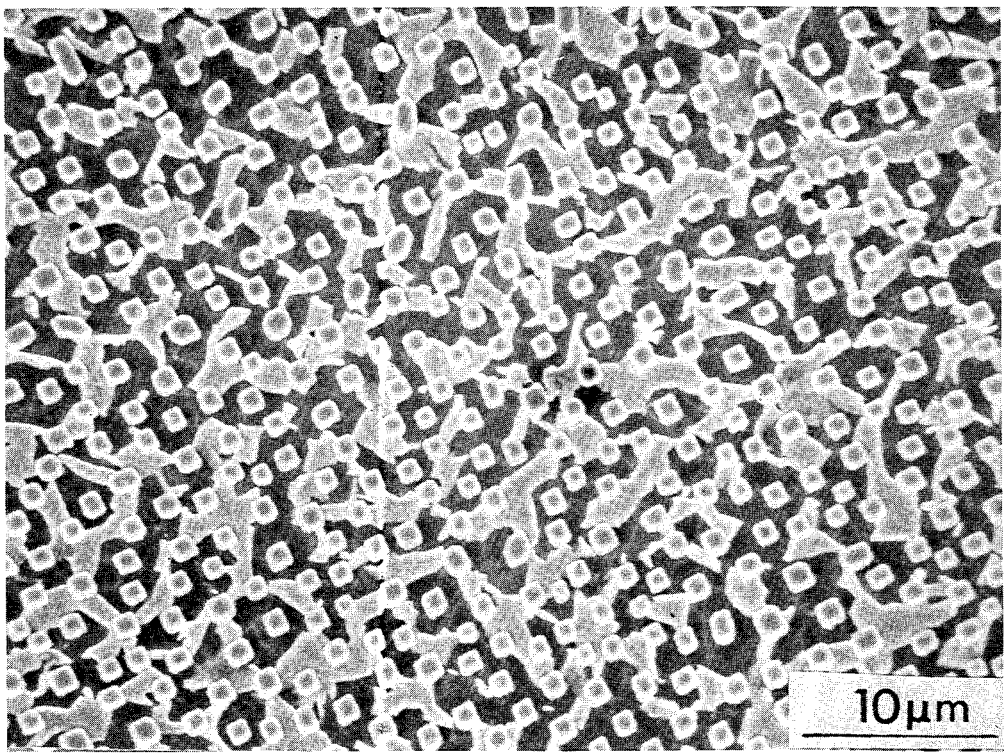

Figure 10. - Transverse Microstructure of Alloy 28:
a) As Directionally Solidified
b) After 150 Thermal Cycles to 1100°C.

These two alloys show a markedly different rupture strength response to cycling. However, the differences in microstructural response to cycling appear to be insignificant. All six alloys showed some agglomeration of the γ-phase network, but no apparent effect on the Mo fiber morphology. Microstructural changes are much less than seen in 1150°C cycling for alloy 1 in NASA Contract NAS 3-19711 [ref. 1]. At this point, there seems to be no correlation between microstructural and rupture strength responses to cyclical exposure.

SELECTION AND EVALUATION OF ADVANCED γ/γ'-α MO ALLOY

The information available after Task-II testing was used to select the alloy for detailed evaluation in Task III. Alloy 39 was eliminated from further consideration because its structure was cellular at a 1 cm/h solidification rate, and this cellularity resulted in poor tensile and rupture properties. The remaining five alloys were nearly equal in both longitudinal and transverse tensile properties. Strength and ductility of each alloy is excellent, both at 750°C and 1100°C.

In structural evaluation, alloy 38 at 1 cm/h had the best aligned microstructure on both longitudinal and transverse rating. Alloy 36 was not cellular, but it was not well aligned. Property data for alloy 37 at 2 cm/h and 1 cm/h left doubt as to the optimum rate for this alloy. Alignment for alloy 28 at 1 cm/h and alloy 7 at 2 cm/h was adequate, but not nearly as good as alloy 38 at 1 cm/h.

Stress rupture properties at 1100°C were best for alloy 36, followed closely by alloy 38 and by alloy 37 at each growth rate. For 750°C, all of the alloys have low rupture strength, so that selection should be made based on the 1100°C properties. Alloys 36, 37, and 38 have the best rupture lives after thermal cycling, and alloy 38 shows the least degradation of the three.

Based on the above comparisons, alloy 38 grown at 1 cm/h was chosen for further evaluation in Task III. Its properties showed the best balance of strength, cyclical stability, and ease of processing. Higher solidification rates may be possible for this alloy. Of the six alloys in Task II, alloy 38 had the highest Al content, and may be expected to have better environmental resistance than the others.

Testing in Task III was planned to cover more of the properties important to alloy selection for aircraft jet engine application. Testing involved microstructural evaluation; creep rupture at 750°C and 1100°C; stress rupture at 750°C, 850°C, 950°C, and 1100°C; transverse stress rupture at 750°C and 950°C; thermal cycling to 1100°C followed by rupture at 750°C and 1100°C; 1000 hours exposure at 750°C and 1100°C followed by rupture at the exposure temperature; tensile tests at 23°C, 600°C, 750°C, 850°C, 950°C, and 1100°C; transverse tensile tests at 750°C and 950°C; and

longitudinal shear tests at 750°C and 1100°C. A number of coated specimens were tested in rupture at 750°C, 950°C, and 1100°C and in tension at 23°C, 600°C, 750°C, 950°C, and 1100°C. Uncoated specimens were heat treated to simulate the coating cycle and then ruptured at 750°C and 1100°C. The incipient melting temperature was also determined for the coated alloy. Dynamic modulus and coefficient of thermal expansion were determined, and the cyclical oxidation behavior of alloy 38 at 750°C and 1100°C was measured. The reactivity of the liquid alloy was measured in three mold materials and two core materials.

Structure and Chemistry of Alloy 38

Four ingots of alloy 38 were directionally solidified at 1 cm/h. The ingots were 4 cm in diameter by 16.5 to 18.8 cm in length. The top half of the alloy 38 ingot that was used in Task II (LDB-298) was also used in Task III. It was decided to use four large ingots for Task III to allow some analysis of ingot-to-ingot variations. The Task III material also represented two master melts.

After directional solidification each ingot was evaluated for microstructure. The microstructural ratings for the Task-III ingots, using the visual standards of Figure 2, are given in Table XIII. Ingots LDB-335 and LDB-341 had a short perturbation just above the Mo sort-out zone, but had good structure above that. Ingot LDB-342, on the basis of the longitudinal stripes, would be rated as the ingot with the least controlled microstructure. The stripe on that ingot was rated as A/B.

TABLE XIII. - STRUCTURE OF TASK-III INGOTS OF ALLOY 38 (AG-170) AT 1 cm/h, 4-cm DIAMETER

DS No.	Total length (cm)	Chill cast (cm)	Mo sort-out (cm)	Structure on longitudinal stripe*
LDB-298	19.0	2.3	0.3	15.3 cm A, 1.1 cm C/D
LDB-327	18.4	1.3	0.1	15.8 cm A, 1.1 cm C/D
LDB-335	18.8	1.2	0.1	0.3 cm A, 0.4 cm C/D, 13.3 cm A, 3.5 cm B/D
LDB-341	16.5	2.7	0.2	0.6 cm A, 0.1 cm D, 8.0 cm A, 1.1 cm B, 0.8 cm C, 3.0 cm D
LDB-342	16.8	2.4	0.3	11.5 cm A/B, 0.7 cm C, 1.9 cm D

*See Figure 2 for structure ratings.

Chemical analysis was performed using x-ray fluorescence. Analysis was performed on transverse sections from the chill-cast zones of ingots LDB-298, LDB-327, and LDB-335 from this contract; a transverse section of the chill-cast zone of a General Electric ingot LDB-332; and a transverse section through the aligned region of LDB-298 at a distance of 1.4 cm above

the top of the Mo zone (which corresponds to a fraction solidified of approximately 0.10). Analysis of the raw data from the chill-cast sections showed that LDB-327, LDB-332, and LDB-335 were approximately the same composition; while LDB-298 was slightly different, particularly in Ni and Mo content. As a result of this, it was decided to use the arithmetic average of the LDB-327, LDB-332, and LDB-335 chill-cast sections as the standard for x-ray fluorescence. Data were collected using 2.2-cm-diameter masks, and three separate runs were performed to check repeatability. The analyses of the composition are presented in Table XIV. The table gives the average, the minimum, and the maximum of the three runs. The repeatability is excellent. The absolute value of the analysis is, of course, only as good as the standard used. The analysis of the aligned section at a fraction solidified, g, of 0.10 would indicate rhenium segregates to the solid and aluminum segregates to the liquid.

TABLE XIV. - X-RAY FLUORESCENCE RESULTS FOR ALLOY 38 INGOTS (AG-170)

Sample	Weight percent				
	Ni Avg/Min/Max	Al Avg/Min/Max	Mo Avg/Min/Max	V Avg/Min/Max	Re Avg/Min/Max
Chill-cast LDB-298	62.88/62.79/63.00	5.98/5.95/6.02	28.37/28.22/28.50	1.64/1.64/1.65	1.22/1.20/1.23
Chill-cast LDB-327	61.40/61.34/61.44	5.82/5.78/5.88	29.92/29.92/29.92	1.65/1.64/1.66	1.21/1.20/1.21
Chill-cast LDB-332	61.63/61.52/61.71	5.96/5.96/5.97	29.59/29.51/29.69	1.65/1.64/1.65	1.19/1.18/1.19
Chill-cast LDB-335	61.56/61.52/61.63	5.86/5.80/5.89	29.71/29.61/29.79	1.66/1.65/1.66	1.21/1.20/1.21
Aligned (g = 0.10) LDB-298	61.41/61.27/61.56	5.69/5.69/5.70	29.71/29.54/29.82	1.66/1.65/1.66	1.54/1.50/1.58
Alloy 38 Nominal	61.53	5.88	29.74	1.65	1.20

Tensile and Shear Properties of Alloy 38

Results of vacuum testing at a nominal strain rate of 0.044 min^{-1} are shown in Table XV for longitudinal and transverse tensile tests. Room temperature tests were performed in air. The yield stress increases to a maximum at about 850°C, while the ultimate strength apparently decreases monotonically with temperature. At temperatures above 750°C, there is very little strain hardening, and maximum loads occur at less than 1 percent plastic strain. Transverse strengths at 750°C and 950°C are almost as high as longitudinal strengths, and transverse ductilities are good, meeting the goals of NASA contract NAS 3-19711.

Results of longitudinal shear tests in vacuum are given in Table XVI. Failure occurred by shear at 50 to 65 percent of the longitudinal and transverse ultimate tensile strengths.

TABLE XV. - TENSILE RESULTS FOR ALLOY 38 (AG-170) AT 1 cm/h (0.044 $min.^{-1}$ in vacuum, except in air at 25°C)

Specimen No.	DS No.	Temperature (°C)	0.2% offset yield strength (MPa)	Ultimate tensile strength (MPa)	Strain to maximum load (%)	Strain to failure (%)	R.A. (%)
			Longitudinal				
T-233	LDB-298-T[1]	25	703	1489	17.	17.	18.
T-247	LDB-342-B	25	745	1503	19.	20.	24.
T-243	LDB-341-T	600	869	1110	13.	18.	37.
T-248	LDB-342-T	600	848	1110	18.	21.	22.
T-229	LDB-298-T	750	958	1034	8.1	19.	42.
T-230	LDB-298-T	750	938	1020	8.1	18.	44.
T-244	LDB-341-T	850	1020	1062	0.89	9.6	17.
T-249	LDB-342-T	850	976	976	0.2	33.	59.
T-245	LDB-341-T	950	632	632	0.20	34.	67.
T-250	LDB-342-T	950	634	634	0.2	34.	64.
T-231	LDB-298-T	1100	430	438	0.82	60.	86.
T-232	LDB-298-T	1100	441	450	0.78	84.2	77.
			Transverse				
T-239	LDB-341-T	750	834	924	6.7	9.5	19.
T-240	LDB-341-T	750	808	896	4.7	5.7	6.0
T-241	LDB-341-T	950	512	590	2.9	6.9	15.
T-242	LDB-341-T	950	542	604	2.8	6.0	6.3

1) T = top, B = bottom of aligned structure

2) Double necking.

3) Failure may be fillet initiated.

TABLE XVI. - LONGITUDINAL SHEAR STRENGTH OF ALLOY 38 (AG-170) AT 1 cm/h (Tested in vacuum at 0.044 $min.^{-1}$)

Specimen No.	Temperature (°C)	Failure stress (σ_F)	$\sigma_F/\sigma_{Long.}$	σ_F/σ_{Trans}
T-257	750	537	0.52	0.59
T-258	750	537	0.52	0.59
T-259	950	357	0.56	0.60
T-260	950	381	0.60	0.64

Stress Rupture and Creep Properties of Alloy 38

The results of longitudinal and transverse rupture testing in argon are listed in Table XVII. The range of lifetimes for duplicate rupture tests is narrower than for conventional superalloys. Four longitudinal creep rupture tests were performed on alloy 38. The data are listed in Table XVIII. The test conditions were chosen to yield failure in 1000 hours. The 750°C/630 MPa test was too severe; the second 750°C test was performed with a stress of 550 MPa. Two tests were run at 1100°C/90 MPa. There is a large difference in time to a given strain between the two 1100°C tests; the second creep test at 1100°C was terminated at 1000 hours, with the sample having crept less than 2 percent.

Effects of Prior Exposure on Stress Rupture Properties of Alloy 38

The results for rupture testing in argon of previously exposed samples of alloy 38 are listed in Table XIX. Machined bars were made from cylinders of the alloy which had been vacuum encapsulated in quartz prior to cyclical or isothermal furnace exposures. Cyclical exposures were one-hour long. Rupture properties for the unexposed alloy are included in the table.

For material cycled or isothermally exposed to a maximum temperature of 750°C, there is little effect on rupture resistance at 750°C. The 150- and 510-hour exposure specimens showed identical rupture lives with a possible 0.2 to 0.5 decrease in the Larson-Miller parameter (C=20, 1.8 x K) from the unexposed life. This is well within the normal scatter for directionally solidified eutectics; thus, it may represent no degradation at all. For the isothermally exposed specimens, one bar was equivalent to the best unexposed test, while the second bar was 0.4 to 0.7 parameters below the unexposed tests. Rather than representing decreased rupture resistance, the spread of a 0.7 parameter probably defines the normal scatter of directionally solidified strength. No microstructural changes were noted after 750°C cyclical or isothermal exposure.

The microstructures for the 1100°C cyclical and isothermal exposures to long times showed the same behavior as reported in section "Thermal Cyclical Effects on Stress Rupture Properties of Task-II Alloys" (page 31); some γ and γ' agglomeration was noted, but no alteration of the Mo fibers was seen. In the 1100°C rupture testing, the material cycled 150 times had lifetimes lower than reported in section "Thermal Cyclical Effects on Stress-Rupture Properties of Task-II Alloys", 54 and 92 hours compared to the previous result of 106 hours. These values were 0.9 parameter or less below the best unexposed life, and one test was superior to one of the two unexposed bars. The results for the bars cycled 510 times were essentially identical to those cycled 150 times. An isothermal exposure for 1000 hours resulted in a 0.3 to 0.9 parameter degradation relative to the unexposed material.

TABLE XVII. - STRESS RUPTURE RESULTS FOR ALLOY 38 (AG-170) AT 1 cm/h (In argon atmosphere)

Specimen No.	DS No.	Temperature (°C)	Stress (MPa)	Time to failure (h)	Elongation (%)	R.A. (%)
		Longitudinal				
1824	LDB-335-B*	750	775	44	32	37
1838	LDB-341-B	750	775	34	25	30
1840	LDB-341-B	850	485	18	30	62
1842	LDB-341-B	850	485	14	48	66
1825	LDB-335-B	950	275	119	53	70
1841	LDB-341-B	950	275	139	32	64
1826	LDB-335-B	1100	125	127	25	73
1839	LDB-341-B	1100	125	70	22	67
		Transverse				
1819	LDB-327-T	750	550	37	4.7	2.0
1830	LDB-335-T	750	550	82	6.0	2.4
1820	LDB-327-T	950	110	88	4.0	1.2
1831	LDB-335-T	950	110	356	6.7	11.6

*B and T designate specimens taken from bottom or top of aligned structure of ingot.

TABLE XVIII. - TASK-III CREEP TESTS OF ALLOY 38 (AG-170) AT 1 cm/h (DS No. LDB-327-B) (In argon atmosphere)

Temperature (°C)	Stress (MPa)	Time (hours) to specified strain 0.02%	0.05%	0.2%	0.5%	1.0%	Time to failure (h)	Elongation at rupture (%)
750	630	<1	<1	7	12	21	184	28
750	550	<1	5	33	91	161	675	25
1100	90	<1	<1	1.5	31	220	756	23
1100	90	<1	<1	10	314	830	>1000	unfailed

TABLE XIX. - LONGITUDINAL STRESS RUPTURE RESULTS FOR ALLOY 38 (AG-170) AT 1 cm/h AFTER PRIOR EXPOSURE

(In argon atmosphere)

		Prior Exposure						
Specimen No.	DS No.	Cycle temperature (°C)	Cycle time (h)	Ingot temperature (°C)	Stress (MPa)	Time to failure (h)	Elongation (%)	R.A. (%)
1845	LDB-335-B(1	750	150	750	775	24	22	42
1855	LDB-335-B	750	510	750	775	26	34	57
1851	LDB-327-B	750(2	1000(2	750	775	41	26	48
1852	LDB-327-B	750(2	1000(2	750	775	18	34	51
1824	LDB-335-B	---	---	750	775	44	32	37
1838	LDB-341-B	---	---	750	775	34	25	30
1835	LDB-335-B	1100	150	750	775	28	24	23
1818	LDB-327-B	1100	500	750	775	7	28	64
1836	LDB-335-B	1100	150	1100	125	92	28	66
1837	LDB-335-B	1100	150	1100	125	54	22	77
1816	LDB-327-B	1100	510	1100	125	43	44	83
1817	LDB-327-B	1100	510	1100	125	87	35	76
1843	LDB-327-B	1100(2	1000(2	1100	125	54	25	71
1844	LDB-327-B	1100(2	1000(2	1100	125	54	25	55
1826	LDB-335-B	---	---	1100	125	127	25	73
1839	LDB-341-B	---	---	1100	125	70	22	67

1) B = bottom, T = top of aligned structure.

2) Isothermal exposure, all others were given cyclic exposures with each cycle consisting of 1 hour at temperatures with intervening cooling to below 300°C.

Material cycled to 1100°C and tested at 750°C showed the largest effect on rupture life. After 150 hours of cycling, a loss of 0.1 to 0.4 parameters was noted, while after 500 hours of cycling the loss was 1.2 to 1.5 parameters, compared to the two unexposed test bars. The microstructural changes may account for this loss in rupture resistance.

Evaluation of Properties of Coated Alloy 38

Coatings 0.013-cm thick of IN-671 (Ni-50 Cr with small amounts of Ti and C) were deposited on pins and test bars of alloy 38 using the low pressure/high velocity plasma spray-coating technique. Incipient melting studies were performed between 1250°C and 1290°C at 10°C increments, with the temperature being held to +0, -5°C. Argon atmospheres were used for the one-hour exposure, and the specimens were helium quenched. As shown in Figure 11, incipient melting occurred in the 1290°C test, but not in any test at 1280°C or below. Due to the temperature tolerances, the incipient temperature is $> 1275°C$, $< 1291°C$.

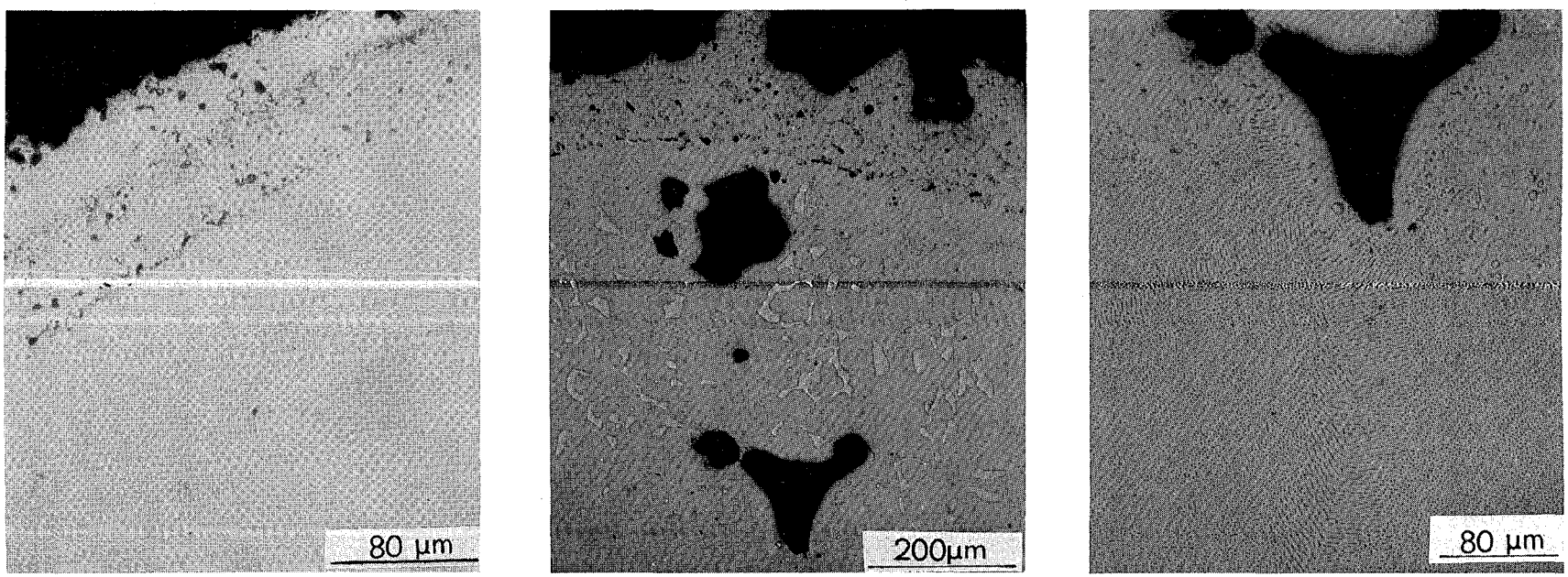

Figure 11. - Microstructures of IN-671-coated Alloy 38 After One-hour Exposures in Argon at a) 1280°C and b) and c) 1290°C.

A diffusion heat treatment was performed on all of the coated test bars: one hour in argon at 1260°C, helium quenched. This heat treatment was chosen to take advantage of the dramatic effect of solution treatment discovered by Henry [ref. 10]. The results of the tensile testing are listed in Table XX. A significant reduction in elongation was noted, especially at the lower test temperatures. Rupture of the coated test bars is listed in Table XXI. Included for comparison are rupture results for uncoated bars given a heat treatment similar to the coated test bars. The 750°C and 1100°C uncoated bars were heat treated at 1275°C, and the 950°C test bar was heat treated at 1260°C.

Thermal Expansion and Dynamic Modulus of Alloy 38

Thermal expansion measurements were performed on a longitudinal pin of alloy 38 machined from ingot DB-335-T which was directionally solidified at 1 cm/h. The test was run from room temperature to 1100°C. The results, showing $\Delta L/L$ and average coefficient of thermal expansion, are given in Table XXII.

Dynamic modulus measurements were performed on a longitudinal pin of alloy 38 machined from ingot DB-342-B which was directionally solidified at 1 cm/h. Measurements were made at room temperature and 100°C increments to 1225°C. The results are shown in Table XXIII. For comparison [refs. 11-13], moduli in the $<100>$ direction at 23°C are 125 GPa for Ni, 99 GPa for Ni_3Al, and 357 GPa for Mo.

Cyclical Oxidation Resistance of Alloy 38

The results of cyclical oxidation testing in static air furnaces are presented in Table XXIV. The cycles were one hour in duration, with 50 minutes in the hot zone of a furnace at 750°C, 1000°C, or 1100°C. Repeatability from specimen to specimen was excellent at all temperatures. For reference, a weight loss of 8.6 mg/cm^2 is approximately equivalent to a 10-μm loss in thickness from all of the surfaces. Heavy yellow growths were present on the 1000°C- and 1100°C-exposed samples. The growth flaked on cooling revealing a black, adherent oxide. A light growth, also yellow, formed on the 750°C-exposed samples, and this layer was more adherent. Metallographic examination of all six specimens indicated there was no preferential oxidation of the matrix or the fiber. The γ-γ' structure of the matrix continued to the interface with the oxide, indicating no significant Al denudation due to protective Al_2O_3 formation.

Casting and Reactivity Studies of Alloy 38

Five casting trials (listed in Table XXV) were run using alloy 38 in various core and mold combinations. Three molds were used: silica bonded-alumina; silica bonded-alumina in an Ar-CO atmosphere, which yielded an

TABLE XX. - LONGITUDINAL TENSILE RESULTS FOR ALLOY 38 (AG-170) AT 1 cm/h

(Coated with IN-671 and Heat Treated*; tests in vacuum, except in air at 25°C)

Specimen No.	DS No.	Temperature (°C)	0.2%** offset yield strength (MPa)	Ultimate tensile strength** (MPa)	Strain to maximum load (%)	Strain to failure (%)	R.A.† (%)
T-265	LDB-342-T	25	1241/1545	1400/1782	2.1	2.1	3.0
T-266	LDB-342-T	600	1165/1440	1200/1475	2.4	2.4	5.3
T-267	LDB-342-T	750	1324/1615	1365/1668	0.8	8.0	18.
T-268	LDB-342-T	950	731/904	731/904	0.3	19.	52.
T-269	LDB-342-T	1100	443/536	457/553	0.8	22.	61.

*Heat treatment was 1 hour at 1260°C in argon, helium quench.

**A/B: "A" calculated from coated diameter, "B" from bare diameter.

†Calculated from coated diameter.

TABLE XXI. - LONGITUDINAL STRESS RUPTURE RESULTS FOR ALLOY 38 (AG-170) AT 1 cm/h

(Coated with IN-671 and Heat Treated*; tests in argon atmosphere)

Specimen No.	DS No.	Temperature (°C)	Stress (MPa)	Time to failure (h)	Elongation (%)	R.A. (%)
1853**	LDB-342-B	750	880	554	5.6 (near fillet)	3.0
1867**	LDB-342-B	950	300	147	29.	58.
1854**	LDB-342-B	1100	125	426	12.	33.
1871†	LDB-342-B	750	880	410	10.	22.
1872†	LDB-342-B	950	300	136	39.	62.
1873†	LDB-342-B	1100	125	199	13.	37.

*Heat treatment was 1 hour at 1260°C in argon, helium quench. Two of the uncoated bars (Nos. 1853 and 1854) were treated at 1275°C.

**Uncoated, included to document the effect of the coating heat treatment cycle.

†Stress calculated using original uncoated diameter.

Temperature (°C)	ΔL/L (10^{-6})	α_m* (10^{-6} °C^{-1})
20	0	--
200	1,650	9.17
400	3,651	9.61
600	5,790	9.98
800	8,001	10.26
1000	10,656	10.87
1100	11,769	10.90

*α_m is average thermal expansion coefficient between room temperature and the temperature of interest

TABLE XXII. LONGITUDINAL THERMAL EXPANSION DATA FOR ALLOY 38 (AG-170) AT 1 cm/h

Temperature (°C)	E_{gd} (GPa)	E_{gd} (10^6 psi)
25	174	25.2
208	177	25.6
290	175	25.4
384	171	24.8
437	165	24.0
500	165	23.9
565	161	23.4
631	161	23.3
712	160	23.2
816	159	23.0
866	148	21.5
915	143	20.7
975	141	20.5
1074	130	18.8
1128	131	19.0
1210	112	16.3

TABLE XXIII. LONGITUDINAL DYNAMIC (SONIC) MODULUS FOR ALLOY 38 (AG-170) AT 1 cm/h (DS No. LDB-342-B)

TABLE XXIV. - CYCLICAL OXIDATION RESISTANCE OF ALLOY 38 (AG-170; DS No. LDB-342-T)

(1 h cycles in static air furnace, two samples for each test)

Cyclical time (h)	Weight change (mg/cm^2)	Weight change (mg/cm^2)
	750°C Exposure	
22	-0.07	-0.04
92	+0.54	+0.52
188	+0.83	+0.85
258	-0.34	-0.10
354	-0.66	-0.13
447	-1.93	-0.97
517	-2.25	-1.07
636	-3.13	-1.34
	1000°C Exposure	
21	-8.95	-10.91
44	-55.87	-52.83
69	---	-91.40
	1100°C Exposure	
25	-76.55	-60.38
34	-79.58	-73.70

TABLE XXV. - CASTING AND REACTIVITY STUDIES OF ALLOY 38 (AG-170)

DS No.	Casting shape	Mold material	Core material	Maximum metal temperature (°C)	Casting rate (cm/h)	Furnace atmosphere
LB-379	High-pressure turbine blade	Al_2O_3-SiO_2	---	1700	1	argon
LB-385	High-pressure turbine blade	Al_2O_3-SiO_2	---	1700	1	argon - 10% CO
LB-381	High-pressure turbine blade	$ZrSiO_4$-SiO_2	---	1550	1	argon
LB-388	High-pressure turbine blade	Al_2O_3-SiO_2	SiO_2	1550	1	argon
LB-386	22mm cylinder	Al_2O_3	Al_2O_3	1700	1	argon - 10% CO

all-alumina protective layer at the metal-mold interface (U. S. Patent 3, 972, 367); and silica bonded-zircon. Two cores were used: silica, and a porous alumina core formulation. For the silica core casting trial and for the zircon mold casting trial, the maximum metal temperature was held to 1550°C. For the other casting trials, the maximum metal temperature was 1700°C.

The castings were sectioned and examined for microstructural alignment and for signs of metal-ceramic reaction. The castings were aligned, except for the edge of the platform, in the blade castings, with no signs of a metal-ceramic reaction for any ceramic combination. Figure 12 shows the uncored alumina silica mold casting, LB-379.

It is concluded that alloy 38 can be grown in turbine blade shapes, at the rate at which the alloy was developed in the laboratory apparatus; and that there is low potential for any metal-ceramic reactions.

a

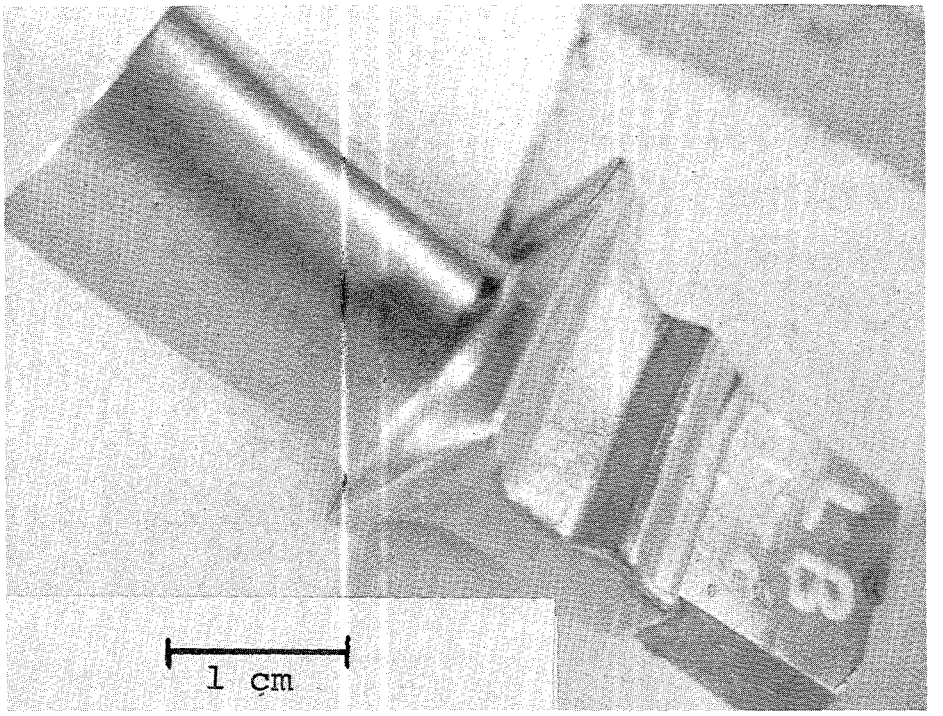

b

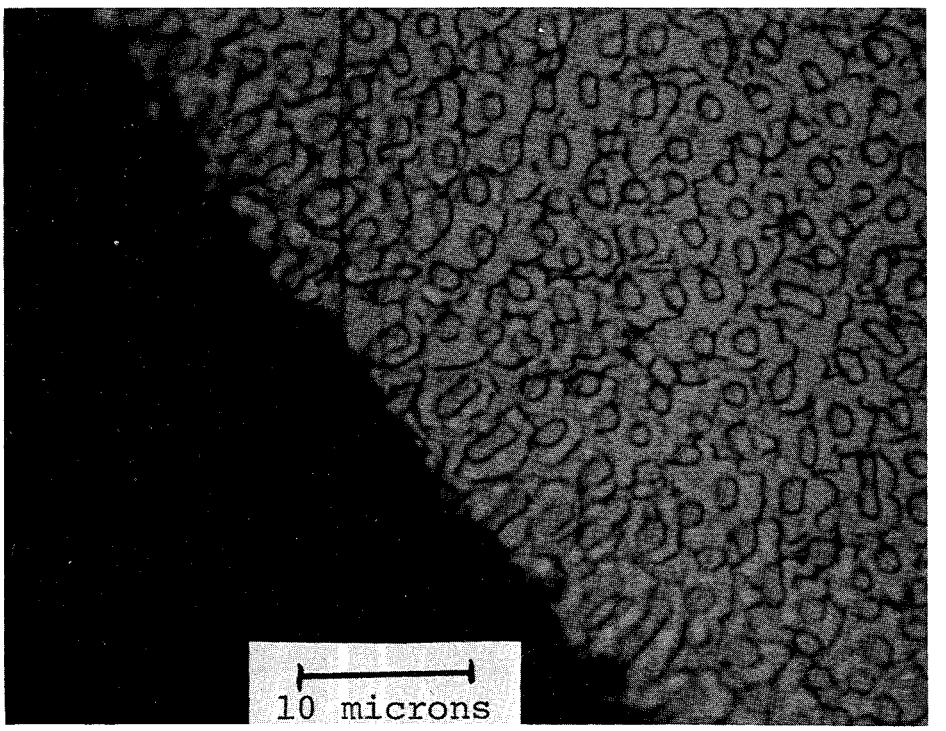

Figure 12. - Alloy 38 Casting DS No. LB-379 Silica Bonded-alumina Mold: a) External Blade; b) As-cast Transverse Section of Metal-mold Interface.

Section 5

DISCUSSION OF RESULTS

On the basis of the results of the Tasks I and II testing programs, alloy 38 was chosen for fuller evaluation. It was judged to be the best on balance of all of the alloys studied. However, it should be remembered that several of the alloys were judged to be nearly equivalent to alloy 38. The likelihood is that a wide range of compositions may be suitable for further development for turbine blade applications. Based on previous results [ref. 1] and the results of Task III, it is believed that much of the behavior of alloy 38 is actually generic to the entire γ/γ'-αMo eutectic system. The discussion which follows, relating to the suitability of alloy 38 as an advanced blade material, should be considered in terms of the general suitability of the γ/γ'-αMo composites for blade applications.

PHYSICAL BEHAVIOR

In Section 2, "Introduction," the properties important in blade design were discussed briefly. Some of the physical properties critical to optimum use of an alloy were moduli of elasticity, coefficients of thermal expansion, and thermal conductivity. These properties determine the thermal strains generated across and along the airfoil. The thermal conductivity of γ/γ'-αMo eutectics is expected to be similar to present generation materials and was not measured in this preliminary evaluation program. However, before such an alloy could be used, this property would have to be documented. The thermal expansion and elastic moduli were expected to be significantly different from currently used materials; therefore, they were measured.

The longitudinal thermal expansion of γ/γ'-αMo eutectics is constrained by the Mo fibers, with the result that the expansion is about 30 percent less than conventional alloys over the service temperature range. This longitudinal expansion behavior will tend to produce lower thermal strains in the temperature gradients present in an operating turbine blade. The low thermal expansion coefficients may be beneficial in decreasing the low-temperature rupture-strength requirement, since the thermal strains are reduced.

The longitudinal elastic modulus measurements show that γ/γ'-αMo eutectics are similar to conventionally cast superalloys, rather than low modulus, directionally solidified alloys. This is largely due to the <100> growth direction being that for the maximum modulus for Mo, but a minimum for γ and γ' [refs. 11-13]. Compared to conventional superalloys, there will be almost no change in the thermal strains due to modulus; but compared to directionally solidified superalloys, the higher longitudinal modulus may tend to increase thermal strains, partially off-setting the gains from reduced thermal expansion.

The expansion and modulus properties of the γ/γ'-αMo eutectic will be beneficial in thermal strain reduction in airfoil applications, relative to conventional superalloys. Compared to directionally solidified superalloys and NiTaC eutectics, the net gains may be smaller due to the greater longitudinal modulus.

MECHANICAL PROPERTIES

A large number of mechanical properties are important in designing the airfoil and the dovetail of a turbine blade (see Section 2), and only some of these properties have been addressed in the present evaluation. For many of these properties, alloy 38 has a clear advantage over conventional alloys; and for some properties, especially for transverse loading, there is a dramatic advantage over the γ/γ'-δ and NiTaC eutectic systems. There are some properties, however, where the system is at a disadvantage. Alloy development will be a critical step in overcoming these deficiencies, if the γ/γ'-αMo system is to find service as a blade material.

Longitudinal and transverse tensile strengths are shown as a function of temperature for NiTaC-13, γ/γ'-δ, AG-60, and alloy 38 in Figure 13. Although the longitudinal strength of alloy 38 is greater than most conventional superalloys, it is weaker over most of the temperature range when compared to the other eutectic alloys. In transverse testing, it is comparable to the base AG-60 and to NiTaC-13. The alloy has the same significant advantage as AG-60 in tensile elongation for the transverse orientation relative to the other eutectic systems. This advantage in transverse ductility for the γ/γ'-αMo eutectics may be important for resistance to transverse fatigue loading.

A comparison of longitudinal tensile shear strength for the different eutectics is shown in Figure 14. The properties of alloy 38 are intermediate between AG-60 and NiTaC-13 and substantially better than γ/γ'-δ. Longitudinal tensile shear at high strain rates is not viewed as a problem for the γ/γ'-αMo system. However, recent work on shear of this system at creep strain rates (refs. 14, 15) suggests the alloy may be substantially weaker than NiTaC-13, and comparable in strength to γ/γ'-δ.

The rupture behavior of alloy 38 is compared to the other eutectics in Figure 15. The alloy in the coated plus coating heat treated condition is more resistant to longitudinal stress rupture than the base AG-60 at all stresses. It is also within ~ 1 parameter of NiTaC-13 at 800 MPa, and is ~ 2 parameters above NiTaC-13 at 100 MPa. In transverse stress rupture, uncoated alloy 38 is comparable to AG-60, providing a significant strength advantage at high stresses.

Exposure of alloy 38 prior to testing appears to produce very small effects on rupture strength. For the 750°C cyclical and isothermal expo-

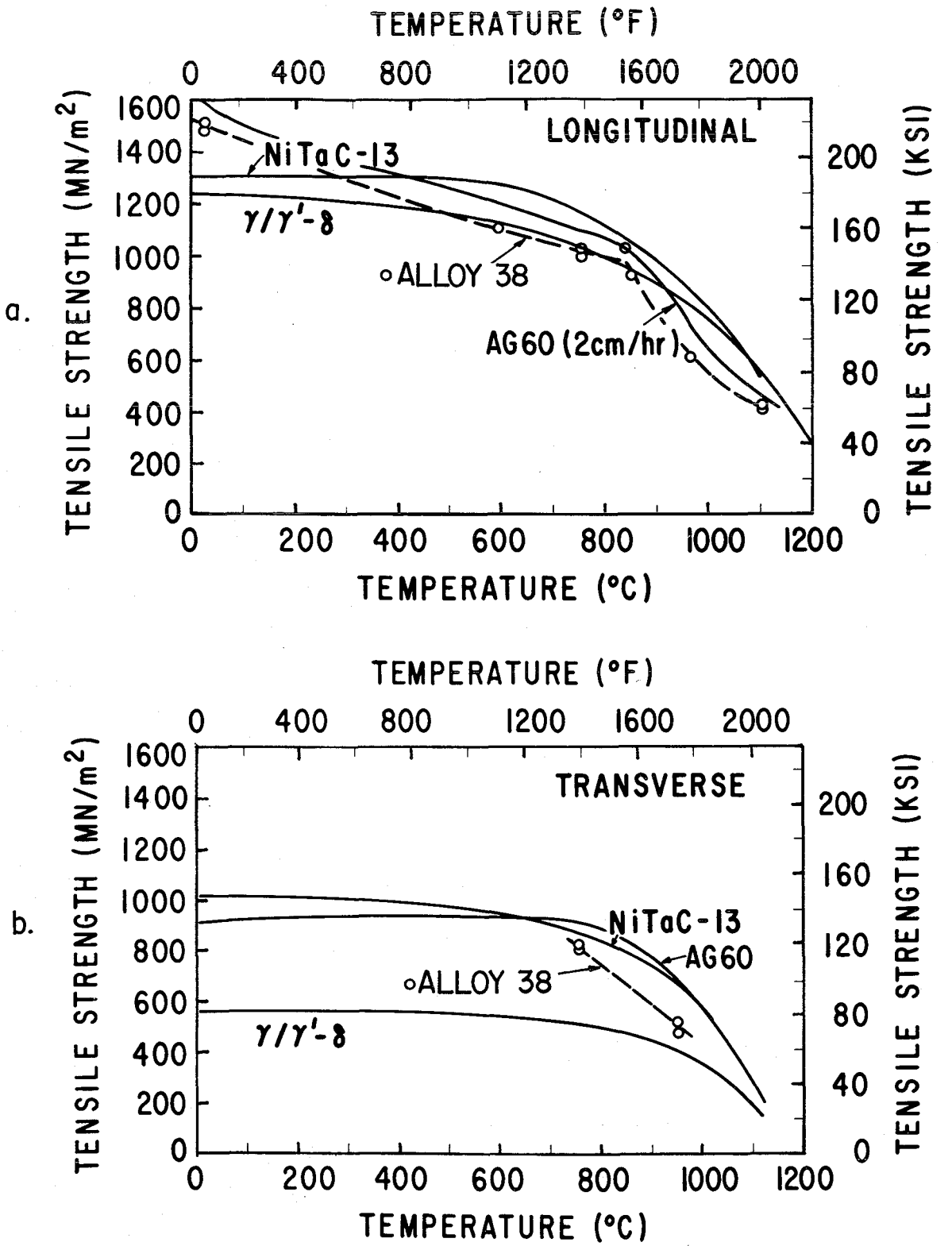

Figure 13. - Tensile Strength of Alloy 38 Compared to Other Eutectics for a) Longitudinal and b) Transverse Orientations.

sures, there appears to be no effect; while for the 1100°C exposures, one-third to one-half of the rupture life may be lost due to exposure. This is a smaller effect than for NiTaC-13 [ref. 16], where two-thirds of the life

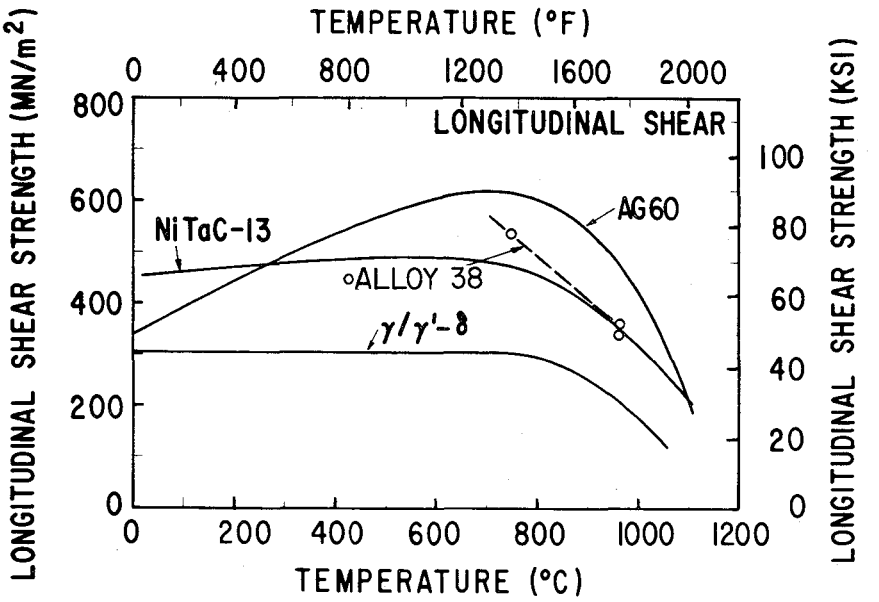

Figure 14. - Longitudinal Shear Strength of Alloy 38 Compared to Other Eutectics.

was lost during comparable 1100°C exposure. The loss is also substantially less than that observed for 1150°C cycling of AG-60. Since in actual blade service only a small fraction of the design life is spent at 1100°C for any portion of the turbine blade, the degradation is small. Compared to conventional superalloys exposed to 1000°C, alloy 38 cycled to 1100°C offers improved stability to rupture life loss during service exposure.

The measurements of resistance to creep deformation for alloy 38 indicate the alloy, and most likely the γ/γ'-αMo system, behaves quite differently from conventional superalloys as well as other directionally solidified eutectics. Their application in turbine blades will require a somewhat different design approach. The alloy NiTaC-13 creeps to 1 percent elongation in about 50 percent of its rupture lifetime, about the same as for conventional superalloys; while for alloy 38 this elongation may occur in as little as 10 percent of its life. This behavior is more like a directionally solidified superalloy than like NiTaC-13 γ/γ'-δ. This behavior can be included in blade design and is not likely to limit the applicability of the γ/γ'-αMo system.

PROCESSING

As [illegible] true with the γ/γ'-αMo base alloy AG-60, alloy 38 (AG-170) prese[illegible] major problems for producing complex, hollow airfoil shapes.

a.

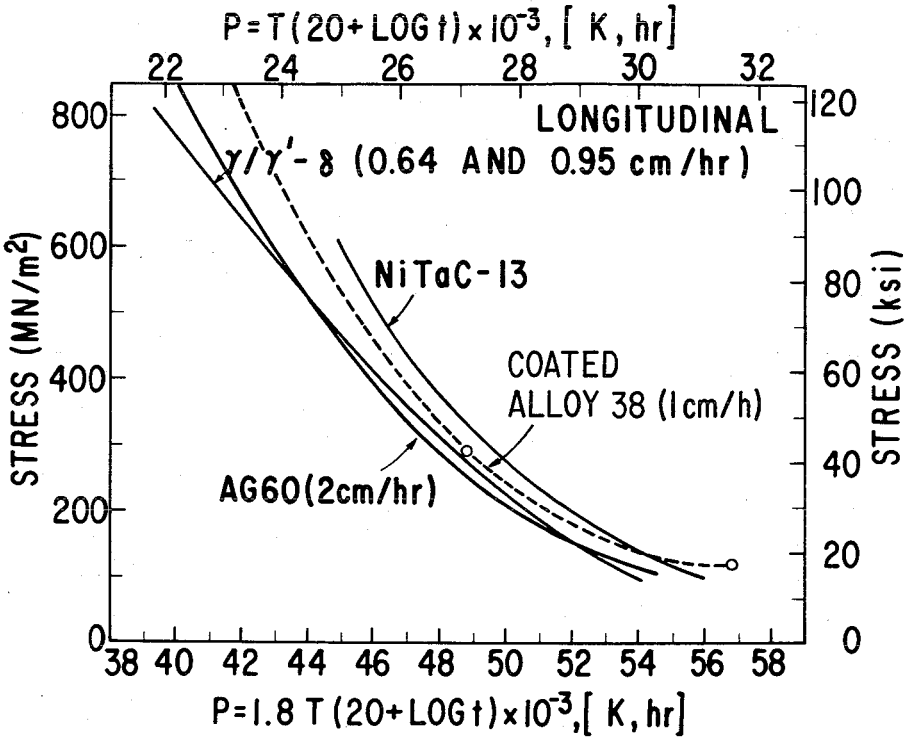

b.

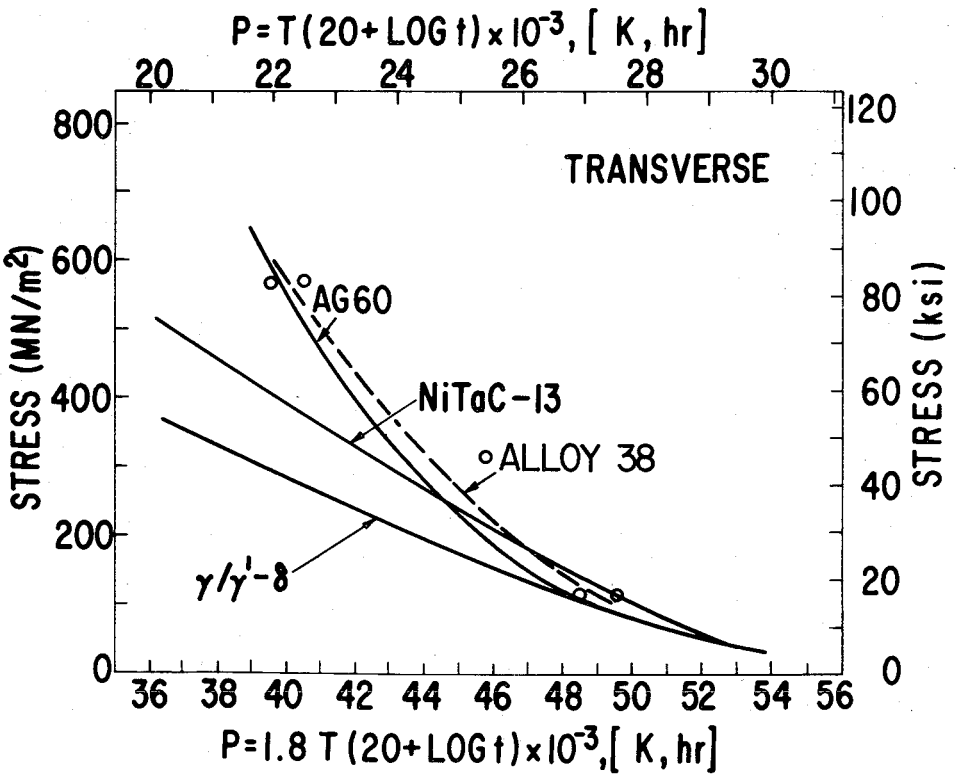

Figure 15. - Rupture Behavior of Alloy 38 Compared to Other Eutectics for a) Longitudinal (IN-671 Coated) and b) Transverse (uncoated) Orientations.

The optimum solidification rate at the blade processing temperature gradients appears to be somewhat less than AG-60, but is greater than both NiTaC-13 and γ/γ'-δ. It should be mentioned that the approach in this program has been to optimize compositions and growth rates at the blade processing gradients so that the properties attained during alloy development can be achieved in the blade shapes. There is a danger that optimization at unrealistically high laboratory gradients may indicate a preference for compositions that cannot be aligned at the blade processing gradients.

Interactions between liquid metal and the ceramic core and mold materials does not present a problem. There appears to be a number of ceramics that will serve as nonreactive materials. As a class of alloys, γ/γ'-αMo eutectics are less tolerant to compositional variation about the nominal than are the NiTaC alloys. Although it is difficult to quantify from the limited experience thus far, closer control on the balance of molybdenum and aluminum must be maintained. Since the sorting-out process is less efficient than in the NiTaC alloys, care must be taken to be near the eutectic trough with the melt composition.

The possibility of a fully aligned structure and a cellular structure both growing in parallel from one solid-liquid interface is cause for some concern. Structures with a rating of 4 to 5 on the transverse sections have greatly reduced 1100°C rupture strength. Nondestructive evaluation techniques will be needed to insure the absence of cellular regions in turbine blade airfoils, since metallographic evaluation of polished airfoil surfaces may miss internal regions of cellularity.

The processing of γ/γ'-αMo eutectics necessarily includes a protective coating deposition. Coatings 0.013-cm thick of IN-671 were deposited on alloy 38 using the low-pressure/high-velocity, plasma spray coating technique. This coating composition was chosen because of the excellent matching of the thermal expansion behavior with that of the substrate. Conventional MCrAlY coatings have higher values of α. For low maximum temperature operation, this coating might have adequate oxidation resistance. However, for high maximum temperature operation envisioned for eutectics, this composition might better serve as an interlayer for an overlaying of a more oxidation-resistant coating, forming a gradation in thermal expansion behavior by appropriate diffusion heat treatments.

Incipient melting between the coating and the substrate can be a severe problem, if it occurs at a temperature within the operating range of the blade. Porosity developed during melting and resolidification can lead to coating spallation very early in blade life. To document whether this might be a problem for alloy 38 and the IN-671 coating, coated pins were subjected to one-hour heat treatments in argon and then helium quenched. This was performed for temperatures of 1250°C to 1290°C, at 10°C increments. The temperature was held to nominal + 0°C, - 5°C. Because of the tolerances

held on the temperature, the incipient melting point must be greater than 1275°C and less than 1290°C. This represents a small decrease from the 1300°C eutectic temperature and is safely outside the expected operating range for eutectic turbine blades.

A diffusion heat treatment is usually specified for plasma sprayed coatings to produce a metallurgical bond across the interface. For this program, the coating heat treatment was chosen to take maximum benefit of the rupture and tensile strength improvements due to heat treatment as discovered by Henry [ref. 10]. The heat treatment chosen was one hour at 1260°C, in order to avoid incipient melting while maximizing the rupture improvement.

The reduction in tensile elongation because of coating and heat-treating the alloy is substantial at low temperature, and less so at high temperature. Heat treatment alone may account for some of this reduction, but the coating is responsible for much of the loss. The eutectic γ/γ'-αMo fails with only a a uniform reduction in cross section (no necking) at low temperatures. If a coated bar develops surface cracks at low strains due to the coating, the γ/γ'-αMo substrate has little resistance to propagation of these cracks. This appears to be a problem only at low temperatures, and the effect possibly may be minimized by optimization of the coating/alloy system. The Ni-50 Cr-50 coatings were uncracked prior to testing.

In rupture testing, it was noted that substantial life improvement occurred for uncoated bars, as a result of the choice of the coating heat-treatment cycle. This behavior was essentially maintained in the coated and heat-treated material.

Finally, the high rate of attack during 1000°C cyclical oxidation must be addressed. Since the cooling passage surfaces may approach 1000°C under certain blade missions, protective coatings may also be required on these internal surfaces.

Section 6

CONCLUDING REMARKS

The present program had as its purpose to improve — through changes in composition — the γ/γ'-αMo alloy AG-60 previously identified as a potential jet engine turbine blade material in NASA contract NAS3-19711. Since the scope of the properties important to blade design is too large to evaluate for a number of alloys, the program was planned to screen a large number of alloys on the basis of rupture resistance alone, select a few alloys for further evaluation, and then choose one alloy for fuller characterization. Properties determined in this characterization included:

- Structure and chemistry
- Longitudinal and transverse tensile behavior
- Longitudinal shear behavior
- Longitudinal stress-rupture and creep resistance
- Transverse stress-rupture resistance
- Effects of prior exposure on stress-rupture
- Tensile and rupture properties after coating deposition
- Thermal expansion
- Dynamic modulus
- Cyclical oxidation resistance
- Liquid metal/mold and core ceramic reactivity

The alloy chosen for this evaluation from among 39 alloys studied was alloy 38 (AG-170), Ni-5.88 Al-29.74 Mo-1.65 V-1.20 Re (weight percent). It was stronger than AG-60 at low stress, high-temperature rupture conditions; and its low temperature rupture strength could be improved beyond that of AG-60 by the proper choice of the coating process cycle. In most of the other mechanical properties evaluated, the alloy was approximately equivalent to or slightly inferior to AG-60. Exposure in the service temperature range had a minimal effect on rupture properties. However, tensile ductility was reduced by the presence of a coating which cracked at low strains during tensile testing. Dynamic modulus behavior was similar to current aircraft blade alloys, but thermal expansion coefficients were significantly smaller than current alloys. This may be beneficial in reducing thermal strains resulting from temperature gradients in turbine airfoils. At the same time, the low expansion behavior may require different coating compositional concepts to achieve a compatible alloy/coating system. The alloy may need a coating on internal cooling passage surfaces as well as on the outer blade surface. The alloy is processable to hollow blade shapes using currently available mold and core ceramics.

On balance, alloy 38 (AG-170) represents an improvement beyond AG-60. Eutectics in the γ/γ'-αMo system should be considered further as possible alternate or superior blade materials in comparison to the NiTaC and γ/γ'-δ eutectic systems. Alloy development is needed to address the problems discussed here, as well as other problem areas such as thermal fatigue and shear rupture. A critical area for study is coating/substrate system development for both internal and external surface environments.

Section 7

REFERENCES

1. Henry, M.F., Jackson, M.R. and Walter, J.L.: Evaluation of Directionally Solidified Eutectic Superalloys for Turbine Blade Applications. NASA CR-135151, 1978.

2. Lemkey, F.D.: Development of Directionally Solidified Eutectic Nickel and Cobalt Alloys. NADC-76115-30, 1975.

3. Pearson, D.D. and Lemkey, F.D.: Creep Rupture, Stability and Fatigue Evaluation of DS Gamma Prime/Gamma-Alpha Eutectic Superalloy. NADC-76342-30, 1978.

4. Smeggil, J.: Coatings for Directionally Solidified Gamma Prime-Gamma Plus Alpha Eutectics. Third Quarterly Progress Report prepared for U.S. Department of the Navy, NAVAIR, Contract No. N000 19-77-C-0424, United Technologies Research Center, East Hartford, Conn., June 1978.

5. Salkeld, R.W., Giamei, A.F. and Taylor, K.E.: Process Evaluation of Directionally Solidified Alpha (Mo) Reinforced Eutectic Turbine Blades. First Quarterly Report prepared for U.S. Department of the Navy, NAVAIR, Contract No. 62269-77-P-0124, Pratt and Whitney Aircraft, Division of United Technologies Corporation, East Hartford, Conn., March 1978.

6. Thompson, E.R. and Lemkey, F.D.: Directionally Solidified Eutectic Superalloys. M11054-2, United Aircraft Corporation, 1973.

7. Ashbrook, R.L.: Directionally Solidified Composite Systems under Evaluation. Paper prepared for Specialists Meeting on Directionally Solidified In Situ Composites, E.R. Thompson and P.R. Sahm, eds., AGARD·CP·156, 1974, pp. 93-115.

8. Henry, M.F.: "Precipitation of γ' in γ-α (Ni-Al-Mo) Eutectics." Scripta Metallurgica, Vol. 10, 1976, p. 955.

9. Cicciarelli, M.F.: Quan-An X-Ray Fluorescence Chemical Analysis Method. Report No. 77CRD060, Corporate Research and Development, General Electric Company, Schenectady, N.Y., 1977.

10. Henry, M.F.: Methods for Improving the Intermediate Temperature Strength of γ/γ'-Mo Eutectics by Heat Treatment. U.S. Patent Pending May 13, 1977.

11. Hearmon, R.F.S.: "The Elastic Constants of Anisotropic Materials-II." Advances in Physics, Vol. 5, 1956, pp. 323-350.

12. Nye, J.F.: Physical Properties of Crystals. Oxford University Press, London, 1967, pp. 131-149.

13. Ono, K. and Stern, R.: "Elastic Constants of Ni_3Al Between 80^{o} and $600^{o}K$," Transactions of the AIME, Vol. 245, 1968, pp. 171-172.

14. Henry, M.F. and Jackson, M.R.: unpublished research. Corporate Research and Development, General Electric Company, Schenectady, N.Y., 1977.

15. Harf, F.H.: Shear Rupture Strength of a Directionally Solidified γ/γ'-α(Mo) Eutectic Alloy. Paper presented at Third International Conference on In-Situ Composites, Boston, Mass., December 1979.

16. Jackson, M.R., Rairden, J.R., and Hampton, L.V.: Coatings for Directional Eutectics. NASA CR-134665, 1974.

DISTRIBUTION LIST FOR NASA CR-159416
Contract NAS3-20383

(The number in parentheses shows how many copies if more than one are to be sent to an address.)

MR. J. ACURIO
MS 77-5
NASA LEWIS RESEARCH CTR.
21000 BROOKPARK ROAD
CLEVELAND, OHIO 44135

DR. C.W. ANDREWS
MS 49-3
NASA LEWIS RESEARCH CTR.
21000 BROOKPARK ROAD
CLEVELAND, OHIO 44135

DR. R.L. ASHBROOK
MS 49-3
NASA LEWIS RESEARCH CTR.
21000 BROOKPARK ROAD
CLEVELAND, OHIO 44135

MR. G.M. AULT
MS 3-5
NASA LEWIS RESEARCH CTR
21000 BROOKPARK ROAD
CLEVELAND, OHIO 44135

MR. C.P. BLANKENSHIP
MS 105-1
NASA LEWIS RESEARCH CTR
21000 BROOKPARK ROAD
CLEVELAND, OHIO 44135

MR. J.C. FRECHE
MS 49-1
NASA LEWIS RESEARCH CTR
21000 BROOKPARK ROAD
CLEVELAND, OHIO 44135

DR. H.R. GRAY
MS 49-3
NASA LEWIS RESEARCH CTR.
21000 BROOKPARK ROAD
CLEVELAND, OHIO 44135

MR. R.W. HALL
MS 49-1
NASA LEWIS RESEARCH CTR
21000 BROOKPARK ROAD
CLEVELAND, OHIO 44135

MR. F.H. HARF (15)
MS 49-3
NASA LEWIS RESEARCH CTR
21000 BROOKPARK ROAD
CLEVELAND, OHIO 44135

MR. M.H. HIRSCHBERG
MS 49-1
NASA LEWIS RESEARCH CTR.
21000 BROOKPARK ROAD
CLEVELAND, OHIO 44135

DR. H.B. PROBST
MS 49-3
NASA LEWIS RESEARCH CTR.
21000 BROOKPARK ROAD
CLEVELAND, OHIO 44135

MR. N.T. SAUNDERS
MS 501-2
NASA LEWIS RESEARCH CTR
21000 BROOKPARK ROAD
CLEVELAND, OHIO 44135

MR. C.M. SCHEUERMANN (3)
MS 49-3
NASA LEWIS RESEARCH CTR.
21000 BROOKPARK ROAD
CLEVELAND, OHIO 44135

MR. R.A. SIGNORELLI
MS 106-1
NASA LEWIS RESEARCH CTR.
21000 BROOKPARK ROAD
CLEVELAND, OHIO 44135

DISTRIBUTION LIST FOR NASA CR-159416 (Cont'd)
Contract NAS3-20383

MR. J.W. WEETON
MS 106-1
NASA LEWIS RESEARCH CTR.
21000 BROOKPARK ROAD
CLEVELAND, OHIO 44135

CHIEF
AFSC LIAISON MS 501-3
NASA LEWIS RESEARCH CTR
21000 BROOKPARK ROAD
CLEVELAND, OHIO 44135

MR. J. GANGLER / RWM
NASA HEADQUARTERS
WASHINGTON, DC
20546

DR. L.A. HARRIS / RTM-3
NASA HEADQUARTERS
WASHINGTON, DC
20546

MR. D. BEELER
AFML/MB
WRIGHT PATTERSON AFB.
OH 45433

MR. T.G. FECKE
AFAPL/TBP
WRIGHT PATTERSON AFB.
OH 45433

MR. N.M. GEYER
AFML/LLM
WRIGHT PATTERSON AFB.
OH 45433

DR. P.J. AHEARN AMXMR-RM
ARMY MATERIALS AND
MECHANICS RESEARCH CTR.
WATERTOWN, MA 02172

MR. J. LANE
SAVDL-EU-TAPP
US ARMY AIR MOBILITY
R&D LABORATORY
FORT EUSTIS, VA 23604

DR. J.C. HURT
ARMY RESEARCH OFFICE
BOX CM
DURHAM, NC 27706

MR. I. MACHLIN AIR-52031B
NAVAL AIR SYSTEMS COMMAND
NAVY DEPARTMENT
WASHINGTON, DC 20361

MR. R. SCHMIDT AIR-52031A
NAVAL AIR SYSTEMS COMMAND
NAVY DEPARTMENT
WASHINGTON, DC 20361

MR. J.W. GLATZ
NAVY DEPARTMENT
NAVAL AIR PROP. TR. CTR.
TRENTON, NJ 08628

MR. M.K. THOMAS
CODE 30231
NAV. AIR DEV. CENTER
WARMINSTER, PA 18974

DISTRIBUTION LIST FOR NASA CR-159416 (Cont'd)
Contract NAS3-20383

MR. J.P. GUDAS
NAVY DEPARTMENT
NAVAL SHIP R&D CENTER
ANNAPOLIS, MARYLAND 21402

DR. B. MCDONALD
CODE 471, ONR
DEPARTMENT OF THE NAVY
ARLINGTON, VA 22217

MR. J.R. LANE
MATERIALS ADV. BD.
NAT. ACAD. OF SCIENCES
2101 CONSTITUTION AVE.
WASHINGTON, DC 20418

DR. C.W. SPENCER
MATERIALS ADV. BD.
NAT. ACAD. OF SCIENCES
2101 CONSTITUTION AVE.
WASHINGTON, DC 20418

MR. H.E. BOYER
AM. SOCIETY FOR METALS
METALS PARK
NOVELTY, OH 44073

MCIC
BATTELLE MEMORIAL INST.
505 KING AVENUE
COLUMBUS, OHIO 43201

DR. A.S. YUE
DEPARTMENT OF METALLURGY
UNIVERSITY OF CALIFORNIA
LOS ANGELES, CALIFORNIA
90024

DR. J.K. TIEN
HENRY KRUMB SCH. OF MINES
COLUMBIA UNIVERSITY
520 WEST 120 STREET
NEW YORK, NY 10027

MR. T.Z. KATTAMIS
SCHOOL OF ENGINEERING
UNIVERSITY OF CONNECTICUT
STORRS, CT 06268

PROF. A. LAWLEY
DEPT. OF METALL. ENGRG.
DREXEL UNIVERSITY
PHILADELPHIA, PA
19104

DR. A.T. CHAPMAN
GEORGIA INST. OF. TECHN.
ATLANTA, GA 30080

DR. D.L. ALBRIGHT
DEPT. MET. & MATL. ENGRG.
ILL. INST. OF TECHN.
CHICAGO, IL 60616

DR. R.A. GOTTSCHALL
UNIVERSITY OF ILLINOIS
URBANA, IL 61801

PROF. J.D. VERHOEVEN
DEPARTMENT OF METALLURGY
IOWA STATE UNIVERSITY
AMES, IOWA 50010

DISTRIBUTION LIST FOR NASA CR-159416 (Cont'd)
Contract NAS3-20383

DR. W. HERTZBERG
DEPT. MET. & MATL. SCI.
LEHIGH UNIVERSITY
BETHLEHEM, PA 18015

DR. W.R. KRAFT
DEPT. MET. & MATL. SCI.
LEHIGH UNIVERSITY
BETHLEHEM, PA 18015

PROF. M.C. FLEMINGS
DEPT. OF METALLURGY
MASS. INST. OF TECHNOLOGY
CAMBRIDGE, MA 02139

PROF. T.H. COURTNEY
MICHIGAN TECHNOLOGICAL
UNIVERSITY
HOUGHTON, MI 48602

DR. S.A. DAVID
DEPT. OF METALLURGY
UNIVERSITY OF PITTSBURGH
PITTSBURGH, PA 15213

PROF. N.S. STOLOFF
RENSSELAER POLYTECHNICAL
INSTITUTE
TROY, NY 12181

DR. B.F. OLIVER
DEPT. CHEM. & MET. ENGRG
UNIVERSITY OF TENNESSEE
KNOXVILLE, TE 37916

DR. R.V. SISSON
WORCESTER POLYTECHNIC
INSTITUTE
WORCESTER, MA 01609

DR. T.T. COURTNEY
UNIVERSITY OF TEXAS
MATLS.SCI. LAB.
AUSTIN, TX 78712

MR. L.J. FIEDLER
AVCO LYCOMING DIV.
550 S.MAIN STREET
STRATFORD, CT 06497

MR. J. WALTERS
AVCO LYCOMING DIV.
550 S. MAIN STREET
STRATFORD, CT 06497

LIBRARY
STELLITE DIVISION
CABOT CORPORATION
1020 W. PARK AVE
KOKOMO, IN 46901

DR. D.R. MUZYKA
CARPENTER TECHNOLOGY CORP
RES. & DEV. CENTER
P.O. BOX 662
READING, PA 19603

MR. H. MORROW
CLIMAX MOLYBDENUM CORP.
1, GREENWICH PLACE
GREENWICH ,CT 06830

DISTRIBUTION LIST FOR NASA CR-159416 (Cont'd)
Contract NAS3-20383

DR. R.F. KIRBY
CHIEF, MATERIALS ENG.
GARRETT AIRESEARCH
402 S. 36TH STREET
PHOENIX, AR 85034

LIBRARY
MATERIALS SCIENCE LAB.W5
DETROIT DIESEL ALLISON
GENERAL MOTORS
INDIANAPOLIS,IN 46206

DR. A. CHALDER
HOWMET
MISCO DIVISION
ONE MISCO DRIVE
WHITEHALL,MICHIGAN 49461

DR. J. BENJAMIN
INTERNATIONAL NICKEL CO.
MERICA RESEARCH LAB
STERLING FOREST
SUFFERN, NY 10901

DR. D.A. PEARSON
ROCKWELL INTERNATIONAL
ROCKETDYNE DIVISION
6633 CANOGA AVENUE
CANOGA PARK, CA 91304

DR. W. SUTTON
SPECIAL METALS
CORPORATION
NEW HARTFORD, N.Y. 13413

LIBRARY
MATERIALS TECHNOLOGY
TRW EQUIPMENT GROUP
23555 EUCLID AVENUE
CLEVELAND,OH 44117

DR. M. HERMAN
DETROIT DIESEL ALLISON DV
P.O. BOX 894
INDIANAPOLIS, IN 46206

MR. E.J. CARROZZA
HOWMET
AUSTENAL-DOVER DIVISION
DOVER, NJ 07801

DR. R.F. DECKER
INTERNATIONAL NICKEL CO.
ONE NEW YORK PLAZA
NEW YORK, NY 10004

DR. L. KAUFMAN
MANLABS, INC
21 ERIE STREET
CAMBRIDGE, MA 02139

DR. G. GARMONG
ROCKWELL INTERNATIONAL
SCIENCE CENTER
THOUSAND OAKS, CALIFORNIA
91360

DR. T. PIWONKA
MATERIALS TECHNOLOGY
TRW EQUIPMENT GROUP
23555 EUCLID AVENUE
CLEVELAND, OHIO 44117

DR. E.A. STEIGERWALD
TRW METALS DIVISION
MINERVA, OH 44657

DISTRIBUTION LIST FOR NASA CR-159416 (Cont'd)
Contract NAS3-20383

DR. F.D. LEMKEY
UNITED TECHNOLOGIES CORP
RESEARCH CENTER
EAST HARTFORD, CT
06108

DR. E.R. THOMPSON
UNITED TECHNOLOGIES CORP
RESEARCH CENTER
EAST HARTFORD, CT
06108

RESEARCH LIBRARY
UNITED TECHNOLOGIES CORP
400 MAIN STREET
EAST HARTFORD, CT
06108

DR. D.N. DUHL
PRATT & WHITNEY AIRCRAFT
UNITED TECHNOLOGIES CORP
400 MAIN STREET
EAST HARTFORD, CT 06108

DR. A.F. GIAMMEI
PRATT & WHITNEY AIRCRAFT
UNITED TECHNOLOGIES CORP
400 MAIN STREET
EAST HARTFORD, CT 06108

DR. M.L. GELL
PRATT & WHITNEY AIRCRAFT
UNITED TECHNOLOGIES CORP
400 MAIN STREET
EAST HARTFORD, CT 06108

DR. K.D. SHEFFLER
PRATT & WHITNEY AIRCRAFT
UNITED TECHNOLOGIES CORP
400 MAIN STREET
EAST HARTFORD, CT 06108

MR. R.A. SPRAGUE
PRATT & WHITNEY AIRCRAFT
UNITED TECHNOLOGIES CORP
400 MAIN STREET
EAST HARTFORD, CT 06108

LIBRARY
WILLIAMS RESEARCH CORP.
2280 W. MAPLE ROAD
WALLED LAKE, MI 48088

M & S DIVISION FILES
MS 49-1
NASA LEWIS RESEARCH CTR
21000 BROOKPARK ROAD
CLEVELAND, OHIO 44135

MR. J.P. MERUTKA
MS 49-3
NASA LEWIS RESEARCH CTR.
21000 BROOKPARK ROAD
CLEVELAND, OHIO 44135

CONTRACTS SECTION B
MS 500-313
NASA LEWIS RESEARCH CTR
21000 BROOKPARK ROAD
CLEVELAND, OH 44135

LIBRARY (2)
MS 60-3
NASA LEWIS RESEARCH CTR
21000 BROOKPARK ROAD
CLEVELAND, OHIO 44135

REPORT CONTROL OFFICE
MS 5-5
NASA LEWIS RESEARCH CTR
21000 BROOKPARK ROAD
CLEVELAND, OHIO 44135

DISTRIBUTION LIST FOR NASA CR-159416 (Cont'd)
Contract NAS3-20383

TECHNOLOGY UTILIZATION
MS 7-3
NASA LEWIS RESEARCH CTR
21000 BROOKPARK ROAD
CLEVELAND, OHIO 44135

LIBRARY
NASA
GODDARD SPACE FLIGHT CTR
GREENBELT, MARYLAND 20771

LIBRARY
NASA
LANGLEY RESEARCH CENTER
HAMPTON, VA 23365

LIBRARY
NASA
MARSHALL SPACE FLIGHT CENTER
AL 35812

TECHNICAL LIBRARY / JM6
NASA
JOHNSON SPACE CENTER
HOUSTON, TX 77058

LIBRARY - ACQUISITIONS
JET PROPULSION LAB.
4800 OAK GROVE DRIVE
PASADENA, CA 91102

LIBRARY
NASA
DRYDEN FLIGHT RES. CTR
P. O. BOX 272
EDWARDS, CA 93523

LIBRARY - REPORTS
MS 202-3
NASA AMES RESEARCH CENTER
MOFFETT FIELD, CA 94035

ACCESSIONING DEPT (10)
NASA SCIENTIFIC & TECHN.
INFORMATION FACILITY
BOX 8757
BALTIMORE, MD 21240

DEFENCE DOCUMENTATION CTR
CAMERON STATION
5010 DUKE STREET
ALEXANDRIA, VIRGINIA
22314

TECHNICAL LIBRARY
AFML/LAM
WRIGHT PATTERSON AFB.
OH 45433

TECHNICAL REPORTS LIBRARY
DOE
WASHINGTON, DC
20545

MR. W.F. BROWN
MS 105-1
NASA LEWIS RESEARCH CTR.
21000 BROOKPARK ROAD
CLEVELAND, OHIO 44135

DR. R.L. DRESHFIELD
MS 105-1
NASA LEWIS RESEARCH CTR.
21000 BROOKPARK ROAD
CLEVELAND, OHIO 44135

DISTRIBUTION LIST FOR NASA CR-159416 (Cont'd)
Contract NAS3-20383

MR. T.K. GLASGOW
MS 49-3
NASA LEWIS RESEARCH CTR.
21000 BROOKPARK ROAD
CLEVELAND, OHIO 44135

MR. S.J. GRISAFFE
MS 49-3
NASA LEWIS RESEARCH CTR
21000 BROOKPARK ROAD
CLEVELAND, OHIO 44135

MR. J.L. SMIALEK
MS 49-3
NASA LEWIS RESEARCH CTR
21000 BROOKPARK ROAD
CLEVELAND, OHIO 44135

DR. D.J. VIECHNICKY AMXMRR
ARMY MATERIALS AND
MECHANICS RESEARCH CTR.
WATERTOWN, MA 02172

MR. J.P. HAMMOND
OAK RIDGE NATIONAL LAB
OAK RIDGE, TN 37830

MR. E. FLINT
DEPT. OF INTERIOR
BUREAU OF MINES
WASHINGTON, DC 20240

MR. F. WOOD
DEPT. OF INTERIOR
BUREAU OF MINES
P.O. BOX 70
ALBANY, OR 97321

DR. B.A. WILCOX
NATIONAL SCIENCE
FOUNDATION
WASHINGTON, DC 20550

DR. G.T. HAHN
BATTELLE MEMORIAL INST.
505 KING AVENUE
COLUMBUS, OHIO 43201

MR. R. BRAGG
DEPT. OF MATLS. & ENGRG
UNIVERSITY OF CALIFORNIA
BERKELEY, CA 94720

PROF. J.E. DAVISON
UNIVERSITY OF DAYTON
RESEARCH INSTITUTE
300 COLLEGE PARK AVE
DAYTON, OHIO 45409

DR. F.H. COCKS
SCHOOL OF ENGINEERING
DUKE UNIVERSITY
DURHAM, NC 27706

DR. R.I. JAFFEE
ELECTRIC POWER RESEARCH
INSTITUTE
BOX 10412
PALO ALTO, CA 94304

MR. W.B. JOHNSTON
GEORGE MASON UNIVERSITY
4400 UNIVERSITY DRIVE
FAIFAX, VA 22030

DISTRIBUTION LIST FOR NASA CR-159416 (Cont'd)
Contract NAS3-20383

PROF. B. AVITZUR
DEPT. MET. & MATL. SCI.
LEHIGH UNIVERSITY
BETHLEHEM, PA 18015

PROF. N.J. GRANT
DEPT. OF METALLURGY
MASS. INST. OF TECHNOLOGY
CAMBRIDGE, MA 02139

PROF. P. WINCHELL
MATL. SCI. & MET. ENG.
PURDUE UNIVERSITY
WEST LAFAYETTE, IN
47906

DR. K.A. JACKSON
BELL TELEPHONE LABS.
600 MOUNTAIN AVENUE
MURRAY HILL, NJ 07974

LIBRARY
CHRYSLER CORPORATION
DEFENSE-SPACE GROUP
P.O. BOX 757
DETROIT, MI 48231

DR. D.L. SPONSELLER
CLIMAX MOLYBDENUM COMPANY
1600 HURON PARKWAY
ANN ARBOR, MICHIGAN 48106

DR. F.M. DUNLEVEY
GOULD LABORATORIES
GOULD INC.
540 EAST 105TH STREET
CLEVELAND, OH 44108

MR. A. STETSON
SOLAR DIVISION
INTERNATIONAL HARVESTER
2200 PACIFIC HIGHWAY
SAN DIEGO, CAL. 92112

DR. H.F. MERRICK
INTERNATIONAL NICKEL CO.
MERICA RESEARCH LAB
STERLING FOREST
SUFFERN, NY 10901

MR. T. MILES
KELSEY HAYES CORPORATION
7250 WHITMORE LAKE ROAD
BRIGHTON, MI 48116

DR. J.F. RADAVICH
MICROMET LABORATORIES
202 SOUTH STREET
WEST LAFAYETTE,
INDIANA 47906

DR. R. KOSSOWSKI
WESTINGHOUSE RESEARCH LAB
BEULAH ROAD
PITTSBURGH, PENNSYLVANIA
15235

End of Document